CATALYZED HYDROGENATION OF NITROGEN AND ETHYLENE ON METAL (FE, PT) SINGLE CRYSTAL SURFACES AND EFFECTS OF COADSORPTION: A SUM FREQUENCY GENERATION VIBRATIONAL SPECTROSCOPY STUDY

by

Staffan Per Gustav Westerberg

Civil. (Royal Institute of Technology) 2000

A dissertation submitted in partial satisfaction of the

requirements for the degree of

Doctor of Philosophy

in

Chemistry

in the

GRADUATE DIVISION

of the

UNIVERSITY OF CALIFORNIA, BERKELEY

Committee in charge:

Professor Gabor A. Somorjai, Chair

Professor Richard J. Saykally

Professor Yuen R. Shen

Fall 2004

Abstract

CATALYZED HYDROGENATION OF NITROGEN AND ETHYLENE ON METAL (FE, PT) SINGLE CRYSTAL SURFACES AND EFFECTS OF COADSORPTION: A SUM FREQUENCY GENERATION VIBRATIONAL SPECTROSCOPY STUDY

by

Staffan Per Gustav Westerberg

Doctor of Philosophy in Chemistry

University of California, Berkeley

Professor Gabor A. Somorjai, Chair

High-pressure catalytic reactions and associated processes, such as adsorption have been studied on a molecular level on single crystal surfaces. Sum Frequency Generation (SFG) vibrational spectroscopy together with Auger Electron Spectroscopy (AES), Temperature Programmed Desorption (TPD) and Gas Chromatography (GC) were used to investigate the nature of species on catalytic surfaces and to measure the catalytic reaction rates.

Special attention has been directed at studying high-pressure reactions and in particular, ammonia synthesis in order to identify reaction intermediates and the influence of adsorbates on the surface during reaction conditions. The adsorption of gases N_2, H_2, O_2 and NH_3 that play a role in ammonia synthesis have been studied on the Fe(111) crystal surface by sum frequency generation vibrational spectroscopy using an integrated Ultra-High Vacuum (UHV) / high-pressure system. SFG spectra are presented for the dissociation intermediates, NH_2 (~3325 cm^{-1}) and NH (~3235 cm^{-1}) under high pressure

of ammonia (200 Torr) on the clean Fe(111) surface. Addition of 0.5 Torr of oxygen to 200 Torr of ammonia does not significantly change the bonding of dissociation intermediates to the surface. However, it leads to a phase change of nearly 180° between the resonant and non-resonant second order non-linear susceptibility of the surface, demonstrated by the reversal of the SFG spectral features. Heating the surface in the presence of 200 Torr ammonia and 0.5 Torr oxygen reduces the oxygen coverage, which can be seen from the SFG spectra as another relative phase change of 180°. The reduction of the oxide is also supported by Auger electron spectroscopy. The result suggests that the phase change of the spectral features could serve as a sensitive indicator of the chemical environment of the adsorbates.

The intermediates were identified by analyzing the SFG vibrational spectra. Additional information was obtained by monitoring the non-resonant SFG signal. Clean Fe(111) is found to have a large SFG non-resonant signal. The magnitude of the non-resonant signal was dependent on the adsorption species; O_2 and N_2 decrease the SFG non resonant signal, while H_2 and NH_3 increase the signal. The change in non-resonant signal is correlated to the change in work function of Fe(111) upon adsorption. Adsorption induced changes in SFG non-resonant signal was used as an indicator of surface conditions and to monitor surface reactions.

Another concern for high-pressure catalytic processes that has been addressed in this work is the deactivation of the catalyst. The CO poisoning effect on the catalytic ethylene hydrogenation reaction on the Pt(111) surface has been examined by SFG vibrational spectroscopy. It was found that a monolayer of CO prevented the adsorption of ethylene on the Pt(111) surface in the presence of high pressure ethylene (up to 35

Torr). In contrast, CO can adsorb on the ethylene pretreated Pt(111) surface by increasing the CO pressure. However, the coasdsorbed ethylidyne molecules weakened CO bonding, which was evident by the red-shift in the vibrational frequency. In the presence of high pressure CO (>0.1 Torr), the catalytic ethylene hydrogenation was poisoned due to a site blocking effect of the CO adsorption. No catalytic reactivity was observed at temperatures lower than the CO desorption temperature (400K). The measured apparent activation energy of the CO poisoned ethylene hydrogenation reaction was about 20.5 kcal/mol.

The use of sum frequency generation has been extended to study heat of adsorption of CO on Pt(111). Carbon monoxide is a player in many important catalytic reactions and heat of adsorption and adsorption geometry are fundamental aspects of its behavior CO adsorption on Pt(111) was studied at temperatures between 373K and 463K in a pressure range of $1x10^{-8}$ to $3x10^{-5}$ Torr. Adsorption isotherms were obtained using sum frequency generation. By correlating the normalized SFG signal to the surface coverage, the obtained isotherms are in satisfactory agreement with Langmuir adsorption, which is suitable for coverages up to a monolayer. Close to saturation coverage the heat of adsorption was determined to 98kJ/mol, which is in close agreement with values obtained by single crystal adsorption calorimetry, low energy electron diffraction (LEED) and temperature programmed desorption (TPD).

Acknowledgements

When I first arrived to Berkeley at the turn of the millennium, I had no idea what to expect. It was my first time west of the Atlantic and obviously my first time in Berkeley. I was completing my master's degree at the Royal Institute of Technology in Sweden and had gotten the opportunity to spend six months at UC Berkeley in Professor Gabor A. Somorjai's group, learning surface science and sum frequency generation spectroscopy. I spent the first night at the Faculty Club on campus, where I woke up to the ringing of the Campanile's bells. That morning I had my first meeting with Professor Somorjai and he made me feel at home right away. Without any delay he integrated me into his group and threw me into the challenging world of science.

The following months were some of the most busy and exciting I had ever experienced. I learned the ropes from a supportive group of graduate students and post docs. I especially want to thank Keith McCrea, Aric Opdahl, Saskia Hoffer, Steve Baldelli and Peilin Chen for their time and effort to show me the ins and outs of how to carry out experiments and do good science. During this time I also met Solette, who has since become my wife. She made my already great stay in Berkeley even better. When I left for Sweden after six months I knew I wanted to come back to pursue my Ph.D. in the same environment.

Over the years as a graduate student I have met and gotten to know a countless number of people who have helped, inspired and motivated me. Here, I have a chance to thank a few of them. First I would like to thank my advisor, Professor Gabor Somorjai. He has taught me a tremendous amount about science and given me much advice that I

will take with me through life. I would also like to express my deepest thanks to Prof. Ulf Karlsson and Prof. Christofer Leygraf from Royal Institute of Technology. Without their guidance and encouragement I wouldn't be here today. In addition they helped me to obtain a prestigious fellowship from Royal Institute of Technology that has supported me through my Ph.D. program the past four years and for that I am thankful. In addition to the co-workers I have already mentioned, I want to add Keng Chou and Chen Wang to the list of people that I have learned from. Keng was a constant support when it came to problems with lasers and optics and Chen worked with me for two years providing much support and interesting discussions. I also want to thank Inger Coble for handling all the administrative issues.

I would especially like to thank Solette. She has always supported and believed in me and I know she will be there for me in the future. I look forward to sharing the rest of my life with her. Last but not least, I want to thank my parents and sister who made me the person I am today.

Table of Contents

List of Figures and Tables

Number

page

Chapter 1. Introduction

Catalytic reactions play an essential role in our lives. Most biological reactions in our bodies are catalytic and catalytic processes also control photosynthesis, which is vital for our survival. Beside the reactions that Mother Nature has provided for us there are many technologically important reactions utilized in the chemical industry that are catalytic reactions. Given the immense importance of catalytic reactions, a tremendous effort to understand the process has been provided by the scientific community.

Catalysis can be defined as an increase in reaction rate in the presence of a material that is unchanged at the end of the reaction. The first observation of the phenomena was reported in the early 19^{th} century when Kirchhoff saw that acids aid the hydrolysis of starch to glucose. Additional observations were soon made, but Faraday was the first to explore the reasons for the increase in reaction rate when he studied the influence of platinum on oxidation reactions. However, it wasn't until 1836 that Berzelius originated the expression "catalysis". From here on much effort was put into the field of catalysis. One particular reaction that pushed both science and technology forward was ammonia synthesis. Ammonia was needed to make fertilizers to feed an increasing population, and to make explosives during the First World War. The first discovery was the use of osmium and uranium as catalysts at high pressure and high temperature to make ammonia. The high-pressure reaction pushed technology and engineering to allow large-scale production. The catalyst was also changed to iron, which was a much cheaper material. In spite of these and many other advances, the science and technology of catalysis remained very much empirical. One way to improve the understanding of how

catalysts work came with the advances of surface science. With ultra-high vacuum techniques it was possible to study heterogeneous catalytic reactions on an atomic scale. The studies were aimed at identifying the active sites where the adsorption, bond breaking and rearrangement take place and to detect reaction intermediates. Model catalysts were largely used to reduce the complexity of the real catalyst and the information was obtained by low-energy electron diffraction (LEED), Auger electron spectroscopy (AES), X-ray photoelectron spectroscopy (XPS), high-resolution electron energy loss spectroscopy (HREELS) and other techniques. [1-5] Although, an astonishing amount of knowledge emerged from these studies they had one major drawback: they were limited to low pressures because of the large mean free path required for the electrons to reach the sample or the detector. The results obtained at low pressures could not easily be extrapolated to actual high-pressure reactions since the surface compositions could be significantly different under these conditions. The next logical step to obtain a better understanding of catalytic reactions was to perform experiments on model catalyst under high pressures. Photon based techniques provided the necessary tool for such studies. Vibrational spectroscopy, such as infrared (FTIR) and Raman have been useful because they provide molecular information of adsorbates on the surface. [5-7] However, one difficulty is that both the bulk material of the catalyst and the gas-phase reactants can interfere with surface measurement. A technique that utilized photons and was surface sensitive was needed. Recently, sum frequency generation (SFG) has fulfilled those requirements and it has been utilized to study a variety of surfaces and interfaces. [8-13] SFG is a non-linear optical process where two beams, one in the infrared and one in the visible, are overlapped on a surface and a third beam is generated with the sum frequency

on the incoming two. By tuning the infrared frequency, while monitoring the intensity of the sum frequency, a vibrational spectrum can be obtained. The vibrational mode has to be both infrared and Raman active, i.e. have a change in dipole and change in polarizability for the process to occur. This requirement is only met in matter with no inversion symmetry, which exclude most bulk materials, and isotropic phases, such as liquids and gases. However, it allows generation of a sum frequency signal from interfaces and surfaces where the symmetry is broken. Hence, the technique has a unique surface sensitivity, and allows studies of catalytic surfaces under high pressure.

The goal of the studies presented in this thesis has been to gain molecular information, in situ, of catalytic reactions and to obtain a better understanding of the process by performing experiments on heterogeneous catalytic systems. Ultimately, a better understanding of the process could lead to an improved industrial process. Several reactions and specific problems have been investigated. Effort has been directed at understanding the catalytic reaction of ammonia synthesis on iron and to identify the reaction intermediates. The influence of ammonia pressure and the presence of oxygen have been investigated for the ammonia decomposition. In addition, it was found that the intensity of the non-resonant SFG signal was an indicator of the surface composition during reaction conditions.

Another concern for high-pressure catalytic processes that has been addressed in this work is the deactivation of the catalyst. Various reactants, intermediates, products or even unexpected foreign atoms and molecules may cover the catalyst's surface during the catalytic reaction. Specifically, the effect of CO poisoning on ethylene hydrogenation on platinum was investigated. It was found that introduction of CO stopped the reaction at

room temperature by blocking the reactive sites. At temperatures above the desorption temperature of CO the reaction proceeded with an increased activation energy.

Carbon monoxide is a player in many important catalytic reactions, either as a product, as in coal gasification, a reactant, as in CO hydrogenation or oxidation, or as a poison as in the reaction mentioned above. Given the importance of CO, much effort has been put in to understand the behavior of CO. Heat of adsorption and adsorption geometry are fundamental aspects of the behavior and the use of SFG, has been extended to study the heat of adsorption of CO on platinum. With SFG heat of adsorption can be measured at high pressure or under flow conditions, which previously created difficulties.

The dissertation has been organized in the following way: chapter 2 is an introduction of the theory of sum frequency generation vibrational spectroscopy and the origin of molecular vibrations. This chapter will serve as a basis to understanding the selection rules for SFG and to analyze the spectra. The experimental setup of SFG and the UHV-high pressure system are described in chapter 3. An in depth characterization of the laser and optical parametric generation and amplification systems are presented here as well as the SFG setup of the optics and detection system. In addition, the UHV-high pressure chamber, that was constructed to allow spectroscopic studies of catalytic reactions at high pressure, is portrayed. Chapter 4 explores the ammonia decomposition and adsorption on iron catalysts. Ammonia synthesis is a technologically important reaction that takes place under high pressure and temperature. The motivation of the study is to elucidate the reaction mechanism at high pressure and to identify the reaction intermediates. Chapter 5 deals with the interpretation of the non-resonant SFG signal from iron surfaces and the change in intensity during adsorption of gas molecules. The

change in intensity provides a means to follow reactions on the surface and a correlation can be made between the change in intensity and changes in the surface electronic structure of the substrate. Chapter 6 discusses the role of CO poisoning for ethylene hydrogenation on Pt(111). Ethylene hydrogenation is a catalytic reaction that is run at high pressures. If CO is present in the feed for this reaction the reaction is severely affected by it. The details of the poisoning of the surface are reported in this chapter. Chapter 7 explores the possibilities to extend the use of SFG to study isotherms. To demonstrate the technique adsorption of CO on Pt(111) is studied and the heat of adsorption is determined. The benefits of using SFG versus other techniques are also discussed. Finally in chapter 8 some conclusions are drawn from previous chapters and the use of SFG as a tool to study high pressure catalytic reactions is discussed.

References:

(1) Somorjai, G.A. "Introduction to Surface Chemistry and Catalysis", John Wiley & Sons, New York, **1994**.

(2) Somorjai, G.A. *Surf. Sci.* **1994,** *299/300*, 849.

(3) Goodman, D.W. *Chem. Rev.* **1995,** *95*, 523.

(4) Ertl, G. *Surf. Sci.* **1994,** *299/300*, 742.

(5) Woodruff D.P.; Delchar, T.A. "Modern techniques of Surface Science", Cambridge University Press, New York, **1986**.

(6) Roberts, N.K. "Fourier Transform Infrared Spectroscopy of Surfaces", In O'Conner, D.J.; Sexton, B.A.; Smart, R.St.C. editors, Surface Analysis Methods in Material Science, Springer Series in Surface Sciences, Volume 23. Springer-Verlag, Berlin, **1992**.

(7) Chabal, Y.J. Surface Infrared Spectroscopy, Surf. Sci. Rep. **1992**, *8*, 211.

(8) Shen, Y. R. *Surf. Sci.* **1994**, *299/300*, 551.

(9) Du, Q.; Superfine, R.; Freysz, E.; Shen, Y.R. *Phys. Rev. Lett.* **1993**, *70*, 2313.

(10) Johal, M.S.; Ward, R.N.; Davies, P.B. *J. Phys. Chem.* **1996**, *100*, 274.

(11) Conboy, J.C.; Messmer, M.C.; Richmond, G.L. *J. Phys. Chem.* **1996**, *100*, 7617.

(12) Shen, R. Y. *Nature* **1989**, *337*, 519.

(13) Buck, M.; Himmelhaus, H. *J. Vac. Sci. Tech. A* **2001**, *19*, 2717.

Chapter 2. Sum Frequency Generation

2.1 Sum Frequency Generation Theory

Sum frequency generation is conceptually easy to understand. Two pulsed laser beams, one in the visible (ω_{vis}) and the other in the infrared (ω_{IR}) are overlapped on a sample and light with the sum of the two frequencies ($\omega_{sum} = \omega_{vis} + \omega_{IR}$) is generated. The process relies on a non-linear optical effect known as sum frequency generation. The intensity of sum frequency light changes if the infrared light is in resonance with a vibrational mode of a molecule on the sample surface. Therefore, scanning the IR frequency results in a vibrational spectrum.

The phenomena of SFG was first time observed [1] and described in theory [2] in the 1960s, but it wasn't until Y.R. Shen developed the experimental technique in the 1980s that SFG vibrational spectra were recorded. [3] The use of SFG as a technique for vibrational spectroscopy has since gained a lot of attention and the theory and phenomena have been described in detail in the literature, [4-11] To comprehend the technique and to analyze the spectra presented in this thesis, a general description of the SFG process is helpful. SFG is a non-linear process, but to understand the basics of SFG it is beneficial to start with linear optics, since almost all the optical phenomena we see around us everyday are governed by linear optics.

A molecule consists of two or more atoms, each with a positive nucleus and associated electrons of negative charge. The separation of the charges allows each atom in the molecule to form a dipole. When the molecule is placed in a weak electrical field

the dipole starts to oscillate. According to classical laws of electromagnetism the dipoles themselves hereby act as sources of electromagnetic radiation. The induced dipole is proportional to the strength of the electrical field, E. In the presence of the field, the dipole, μ, is given by

$$\mu = \mu^0 + \alpha E \tag{2.1}$$

where μ^0 is the static dipole and α is the polarizability. Since the induced dipole is not, in general, in the same direction as the electric field, α is represented by a (3 x 3) tensor.

In condensed phases it is more convenient to consider the dipole moment per unit volume, or polarization, P. In an electric field

$$P = P^{(0)} + \varepsilon_0 \chi^{(1)} E \tag{2.2}$$

where the linear susceptibility, $\chi^{(1)}$, takes the place of the polarizability and ε_0 is the permittivity in vacuum. Since only a few materials have a static polarizability, the term $P^{(0)}$ can be neglected. For a simple molecular material, the susceptibility depends on the number of molecules per unit volume, N, multiplied by the molecular polarizability averaged over all the orientations of the molecules in the material,

$$\chi^{(1)} = N < \alpha > / \varepsilon_0 \tag{2.3}$$

The linear properties of an isotropic material are characterized by the complex refractive index, n. The refractive index is related to the susceptibility by

$$n = \sqrt{1 + \chi^{(1)}} \tag{2.4}$$

The real part of n determines the speed of light in a medium,

$$v = c / \mathrm{Re}(n) \tag{2.5}$$

and the imaginary part of n determines the absorption coefficient,

$$\alpha = \frac{4\pi}{\lambda_0} \mathrm{Im} \sqrt{1 + \chi^{(1)}} \tag{2.6}$$

where λ_0 is the wavelength of light in vacuum.

With the evolution of lasers the light became more intense. The created electric fields are comparable to the fields felt by an electron in a molecule. The response of the electrons to the field is no longer linear and higher order terms in E must be included in the expression for the dipole moment.

$$\mu = \mu^0 + \alpha E + \beta : EE + \gamma \vdots EEE + ... \tag{2.7}$$

where β and γ are the first and second hyperpolarizabilites. The notation β:EE denotes $\sum_{j,k} \beta_{ijk} E_j E_k$. The corresponding expression for the polarization is

$$P = \varepsilon_0 (\chi^{(1)} E + \chi^{(2)} : EE + \chi^{(3)} \vdots EEE + ...) \tag{2.8}$$

The second order susceptibility, $\chi^{(2)}$, is a third rank tensor and the third order susceptibility, $\chi^{(3)}$, is a tensor of rank 4. They are generally much smaller than $\chi^{(1)}$ and can therefore be neglected when the electrical field is weak, less than 10^6 V/m. Optical processes that arise from $\chi^{(2)}$ and $\chi^{(3)}$ are know as second or third order non linear processes. One consequence of the higher order terms in eq. 2.8 is that the frequency of light can change. Consider an electrical field of the form $E = E(r)\cos\omega t$ in a material in which $\chi^{(2)}$ is non-zero. $P^{(2)}$ is then given by

$$\begin{aligned} P^{(2)} &= \varepsilon_0 \chi^{(2)} : EE = \varepsilon_0 \chi^{(2)} : E(r)E(r)\cos^2 \omega t \\ &= \varepsilon_0 \chi^{(2)} : E(r)E(r)(1 + \cos 2\omega t) \end{aligned} \tag{2.9}$$

The first term in the bracket represents a static electrical field in the material, the second term a dipole oscillating at 2ω, twice the frequency of the incident light. This oscillating dipole can emit light at the frequency 2ω, a process known as second harmonic

generation, SHG. If two laser beams with frequencies, ω_1 and ω_2, are present simultaneously in the material then additional terms appear in the expression for $P^{(2)}$ of the form.

$$\begin{aligned} P^{(2)} &= \varepsilon_0 \chi^{(2)} : E_1(r) E_2(r) \cos\omega_1 t \cos\omega_2 t \\ &= \frac{1}{2} \varepsilon_0 \chi^{(2)} : E_1(r) E_2(r) [\cos(\omega_1 + \omega_2)t + \cos(\omega_1 - \omega_2)t] \end{aligned} \tag{2.10}$$

There are now dipoles oscillating at frequencies ($\omega_1 + \omega_2$) and ($\omega_1 - \omega_2$), which gives rise to SFG and difference frequency generation, DFG, respectively. In SFG vibrational spectroscopy, ω_1 is usually chosen to be in the visible range of the spectrum, while ω_2 is in the infrared. A common geometry for the setup is shown in figure 2.1 where the IR and visible beams are incident from the same direction.

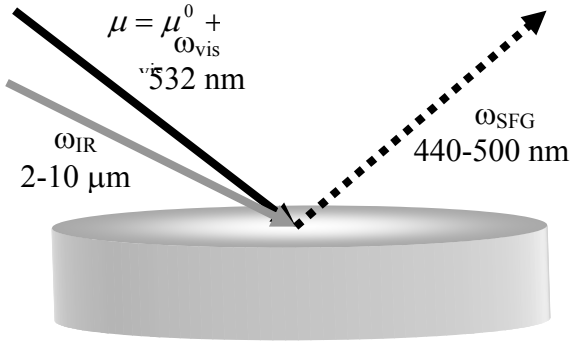

Figure 2.1. Schematic illustration of SFG from an interface. Laser beams with frequencies ω_{vis} and ω_{IR} are overlapped at an interface. Light at frequency $\omega_{sum} = \omega_{vis} + \omega_{IR}$ is emitted at an angle that conserves momentum.

In general, radiation can appear in all directions, however, the sum frequency radiation is strongly peaked in one direction determined by phase matching conditions. For efficient energy transfer from the ω_{vis} and ω_{IR} to the sum frequency ω_{sum} both energy and momentum conservation must be satisfied. The energy conservation requires $\omega_{sum}=\omega_{vis}+\omega_{IR}$, while the momentum conservation requires

$$\boldsymbol{k}_{sum} = \boldsymbol{k}_{vis} + \boldsymbol{k}_{IR} \tag{2.11}$$

Using the conservation of momentum and the angle of incidence for the visible and infrared beams the angle of the sum frequency radiation can be calculated according to eq. 2.12

$$k_{sum} \sin\theta_{sum} = k_{vis} \sin\theta_{vis} + k_{IR} \sin\theta_{IR} \tag{2.12}$$

k_{vis}, k_{IR} and k_{sum} are the three wavenumbers $(2\pi/\lambda)$, θ_{vis} and θ_{IR} are the angles of incidence, compared to the surface normal, of the visible and the IR lasers, and θ_{sum} is the angle of the sum frequency light. Notable is that the angle of emission changes as ω_{IR} is scanned through the spectrum.

An expression for $\chi^{(2)}$ can be found by second order perturbation theory as an infinite sum over the quantum states of the system. [4] The general solution is complicated but it reduces to a simpler system if neither ω_{IR} nor ω_{sum} is in resonance with an electronic dipole transition in the material and only electric dipole transitions are considered. In general, the sum frequency signal is proportional to the square of the effective second order non-linear susceptibility, $\chi^{(2)}_{eff}$ as given by given by Eq. 2.13. For vibrationally resonant SFG, $\chi^{(2)}_{eff}$ can further be described by Eq. 2.14

$$I(\omega_{sum}) \propto \left|\chi^{(2)}_{eff}\right|^2 \tag{2.13}$$

$$I(\omega_{sum}) \propto \left| \chi_{NR} + \sum_q \frac{A_q e^{i\theta_q}}{\omega_{IR} - \omega_q + i\Gamma_q} \right|^2 \qquad (2.14)$$

where χ_{NR} contains the non-resonant contributions to the measured intensity and A_q is the vibrational mode strength. The second term in Eq. 2.14 is maximized when the frequency of the IR beam, ω_{IR}, is tuned near a vibrational mode, ω_q, of one of the surface species. Γ_q is the damping term and θ_q is the relative phase between the *q*th vibrational mode and the non-resonant signal. Eq. 2.14 shows that the profile of a SFG resonance consists of three parts. The first part is a pure background contribution from $\left|\chi^{(2)}_{NR}\right|^2$. The second part comes from interference between each resonant mode and χ_{NR}. The third part includes contributions from individual resonant modes and interference between them. Only if χ_{NR} is negligibly small and the resonances are far apart, will unequivocal resonant peaks appear in the SFG spectrum. Usually the observed spectrum needs to be fit to Eq. 2.14 in order to deduce the characteristic parameters of the resonances, ω_q, A_q and Γ_q, the non-resonant term,χ_{NR}, and the phase θ_q. For single resonant SFG the resonant amplitude A_q is real, however, χ_{NR} can be complex if ω_{sum} approaches resonance surface electronic states. The magnitude and phase of χ_{NR}, relative to A_q, deduced from the fit can therefore carry information about the electronic structure of an interfacial layer.

In analogy with Eq. 2.3 the resonant part of the non-linear susceptibility can be obtained by averaging the hyperpolarizability, β over all the orientations of the molecules.

$$\chi^{(2)}_{R} = N\langle\beta\rangle / \varepsilon_0 \qquad (2.15)$$

Near a vibrational transition, ω_q, in a molecule the hyperpolarizability, β, is given by

$$\beta_{lmn}(\omega_{sum}) = -\frac{1}{2\hbar}\sum\left\{\frac{\langle g|\mu_l|s\rangle\langle s|\mu_m|v\rangle}{\hbar(\omega_{sum}-\omega_{sg})}-\frac{\langle g|\mu_m|s\rangle\langle s|\mu_l|v\rangle}{\hbar(\omega_{vis}+\omega_{sg})}\right\}\times\left\{\frac{\langle v|\mu_n|g\rangle}{\omega_{IR}-\omega_q+i\Gamma}\right\} \quad (2.16)$$

where $|g\rangle$ is the ground state, $|v\rangle$ the exited vibrational state, $|s\rangle$ any other state, Γ^{-1} the relaxation time of the excited vibrational state, and $\boldsymbol{\mu} = e\mathbf{r}$ is the electric dipole operator. Equation 2.16 has a simple physical interpretation. The first term may be identified as the Raman transition dipole moment, and the second term, $\langle v|\mu_n|g\rangle$, as the IR transition dipole moment. Therefore, a molecular vibration has to be both IR and Raman active in order to be SF active, as depicted in figure 2.2

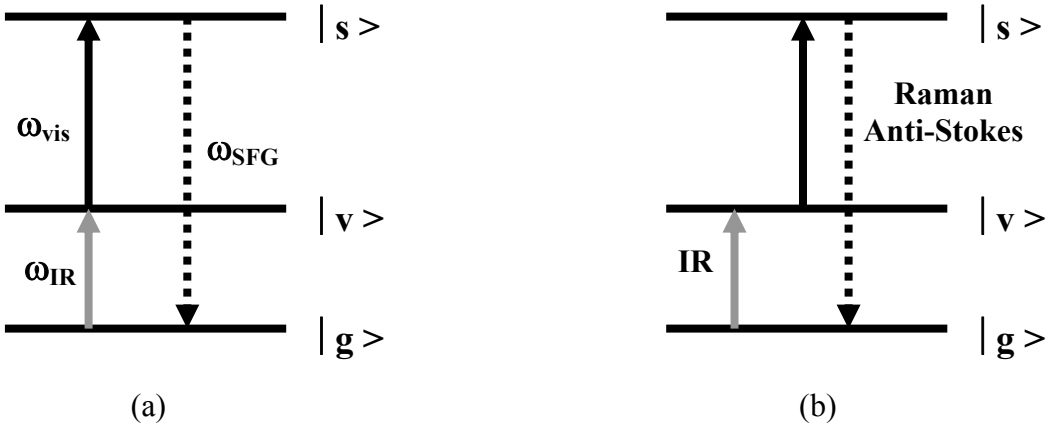

Figure 2.2. Schematic energy level diagram for SFG. (a) Excitation by an IR and a visible photon followed by an emission of a sum frequency photon to relax to the ground state. (b) The SFG process consist of an IR and a Raman transition.

The symmetric properties of $\chi^{(2)}$ forbid SFG in a centrosymmetric crystalline solids by purely electric dipole mechanisms. $\chi^{(2)}$ is a polar tensor of rank three, which changes sign under inversion; $\chi^{(2)}(r) = -\chi^{(2)}(-r)$. However, centrosymmetric crystals are

invariant under inversion operation, and therefore $\chi^{(2)}(r) = \chi^{(2)}(-r)$. This can only be true under the condition that $\chi^{(2)}$ is zero. These symmetry properties have wide implications for SFG spectroscopy. SFG does not occur by electrical dipole mechanisms in gases, liquids or in the majority of solids. SFG only occurs in non-centrosymmetric solids and at surfaces or interfaces, where the symmetry is broken. A result of this interfacial selectivity is that molecules at a surface can be distinguished from a vast excess of the same molecules in solution. The key feature of molecules at an interface that differentiates them from molecules in solution is polar orientation. $\chi^{(2)}$ depends on the polar angle, θ, of a functional group only through the average $\langle \cos\theta \rangle$ and $\langle \cos^3\theta \rangle$. In random orientated molecules these cancel out but an interface imposes a net polar orientation and $\chi^{(2)}$ is nonzero and SFG can occur. Consequently, the magnitude of $\chi^{(2)}$ is very sensitive to the degree of orientational order.

In general, the surface susceptibility $\chi^{(2)}$ is a 27-element tensor, however, it can often be reduced to several non-vanishing elements by symmetry constraints. Interfaces as well as liquid surfaces and monolayer on surfaces are isotropic in the plane of the surface. The symmetry constraints for an in-plane isotropic surface reduces $\chi^{(2)}$ to the following four independent nonzero elements

$$\chi^{(2)}_{zzz}; \chi^{(2)}_{xxz} = \chi^{(2)}_{yyz}; \chi^{(2)}_{xzx} = \chi^{(2)}_{yzy}; \chi^{(2)}_{zxx} = \chi^{(2)}_{zyy} \qquad (2.17)$$

where z is defined to be the direction normal to the surface. These four independent elements contribute to the SFG signal under four different polarization conditions SSP, SPS, PSS, and PPP where the polarization are listed in order of decreasing frequency (sum, vis, IR). P polarization stands for a polarization where the electrical field vector is parallel to the plane of incidence, which contains the surface normal and the incident

beam. In S-polarization the vector is perpendicular to the plane of incidence, see figure 2.3. Which vibrational modes are present under a certain polarization condition depends on the polarization of the IR field and the direction of the IR and Raman transition moments. The SSP polarization has access to vibrational modes with transition moments that have components perpendicular to the surface plane whereas the SPS and PSS polarization conditions access modes that have transitions moments with components parallel to the surface plane. The intensity under PPP polarization contains modes from all of the tensor elements. Vibrational modes with components both perpendicular and parallel to the surface plane will be present in the PPP polarized SFG spectra.

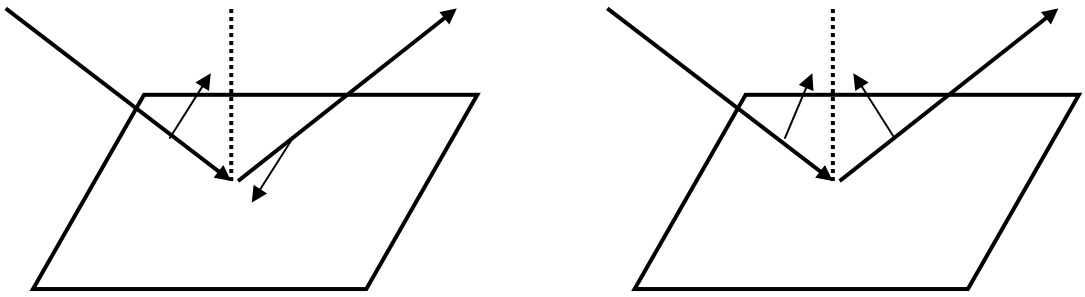

Figure 2.3. (a) S-polarized light reflected on a metal surface. S-polarized light has the electrical vector perpendicular to the plane of incidence. Upon reflection the phase changes 180° and they cancel out each other. (b) P-polarized light reflected on a metal surface. P-polarized light has the electrical vector parallel to the plane of incidence. Upon reflection the phase changes 90° and the sum of the electrical vectors is reinforced.

When doing spectroscopy on metals the choice of polarizations are more limited. Since metals are highly reflective in the IR, the incident and reflected electric

fields in the x and y direction virtually cancel, while those in the z direction add constructively, see fig 2.3. Therefore $\chi^{(2)}_{xzx}$ and $\chi^{(2)}_{zxx}$ are much smaller than $\chi^{(2)}_{xxz}$ and $\chi^{(2)}_{zzz}$, and only the latter are significant. This means that the polarizations available for metals are SSP and PPP. Another way to describe the selection rules of metals is to see it on a molecular level. A unique property of metals is the freedom of the conduction electrons to respond to an electrical field. A charge above the surface of a metal produces lines of force as if there was a negative charge at an equal distance below the surface, an image charge. Dipoles parallel or perpendicular to the surface of the metal will in the same way produce image dipoles, as shown in figure 2.4.

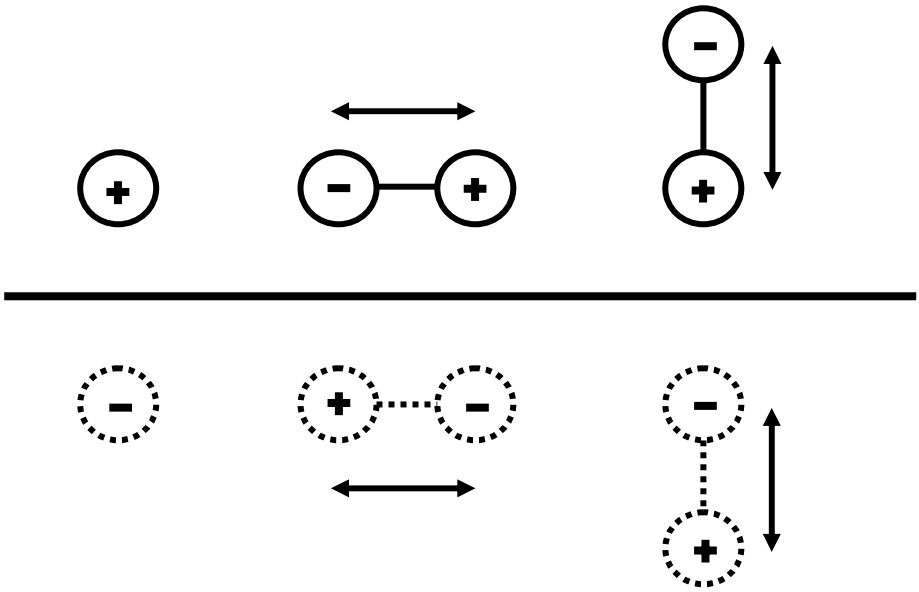

Figure 2.4. (a) The electrical image resulting from a positive charge over the surface. (b) The changes during the vibration of a dipole parallel to the surface of the metal. The image dipole change is in the opposite direction to the original. (c) Changes during the vibration of a dipole perpendicular to the surface. The image dipole is in the same direction as the original dipole.

Because of the separation between the original dipole and its image is of the order of molecular dimensions, (a few Ångströms), which is much smaller than the wavelength of the emitted sum frequency radiation, (about 5000Å), the effect of the image dipole vibration cancel out the dipole vibration originated in the vibrating molecule parallel to the surface. On the other hand the oscillating dipole perpendicular to the surface will be reinforced by the oscillating image dipole.

2.2 Molecular Vibration Theory

Sum frequency generation is only possible if the vibrational mode is both IR and Raman active. In this section IR and Raman spectroscopy will be discussed to give a better understanding for the vibrational spectra obtained by SFG.

There are basically two types of IR spectroscopy, emission or absorption spectroscopy. In absorption light of all different frequencies passes through a sample and the transmitted light is measured at each frequency. In emission the IR is tuned and the reflection off a sample is measured at the corresponding frequency. At frequencies corresponding to a vibrational energy of the sample, some light is adsorbed and less light is transmitted (or reflected) than at frequencies that do not correspond to a vibrational energy of the molecule.

In Raman spectroscopy, light scattered by the sample is observed. Light of a single frequency, ν, is directed onto the sample. Some of the light, about 1/1000 of it, is scattered elastically in all directions. This is called Rayleigh scattering. A small fraction of the scattered light, called Raman scattering, does not have the frequency ν. Instead it

has frequency $\nu \pm \nu_0$, which is an inelastic scattering called Stokes and Anti-Stokes radiation respectively, see figure 2.5. Here, the frequency $\nu \pm \nu_0$ corresponds to a vibrational energy for the molecule.

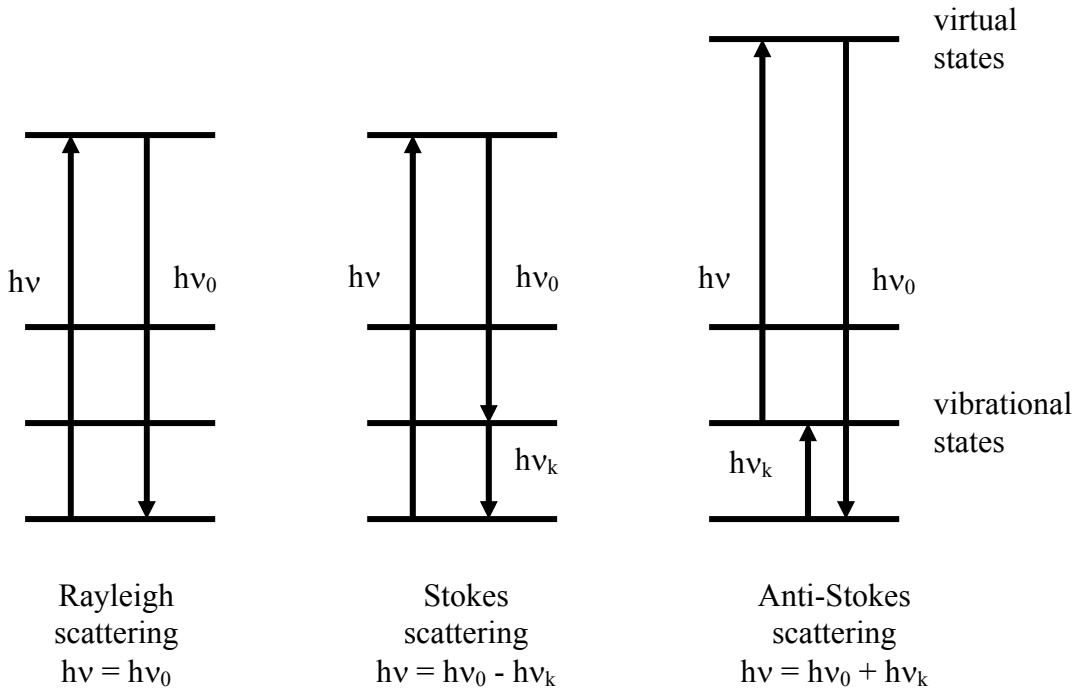

Figure 2.5 Rayleigh and Raman scattering processes.

To understand why these phenomena occur we need to describe what happens on a molecular level. If two particles of charges +e and –e are separated by a distance of r, the permanent electric dipole moment, μ, is given by

$$\mu = er \qquad (2.18)$$

In order to see what magnitude of dipole moment we can expect consider a proton and en electron separated by 1Å, a typical molecular dimension. The dipole moment would be c = (1.602 x 10^{-19} Coulomb) x (10^{-10} m) = 1.602 x 10^{-29} Coulomb m. A commonly used unit is 1 esu, which corresponds to $3.34*10^{-10}$ Coulomb. The dipole moment would then be $4.803*10^{-18}$ esu cm or 4.803 Debye.

Heteronuclear diatomic molecules must have a dipole moment since one atom will be more electronegative than the other and will have a net negative charge. Homonuclear diatomic molecules cannot have permanent dipole moment since both nuclei attract the electrons equally. Polyatomic molecules with a center of inversion will not have a dipole moment whereas non-centrosymmetric will usually have $\mu \neq 0$. Consider a vibrating molecule with a dipole moment. The dipole also oscillates as the atoms move back and forth. This oscillating dipole can adsorb energy from an oscillating electric field only if the field has the same frequency. This is called the resonance frequency, which is characteristic for each molecule, and therefore you can obtain molecular information from an IR spectrum. The selection rule for IR spectroscopy can now be summarized. A vibrational transition is IR active if the dipole moment of the molecule changes during the vibration. The vibration can have different modes as exemplified by a CO_2 molecule in figure 2.6.

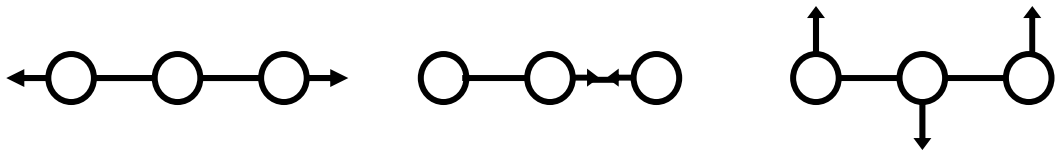

(a) (b) (c)

Figure 2.6. Normal modes of vibration of CO_2. (a) symmetric stretch, (b) asymmetric stretch and (c) bending.

In the case of CO_2, which is a linear molecule, the dipole moment does not change during the symmetric stretch and it is therefore not IR active. For the asymmetric stretch, illustrated in figure 2.6a, there is a change in the dipole moment and it is IR active. Normally the asymmetric stretch has a higher energy than the symmetric stretch. The third mode for the CO_2 molecule shown in figure 2.6c is the bending mode. The energy for bending modes generally falls below the energies of stretching modes. For more complex molecules there are other modes, like wagging, rocking and twisting. So far only the fundamental transitions, i.e. transitions from the ground state to the first excited state, have been considered. There are, however, other possible transitions. An overtone occurs when a mode is excited beyond the first level by a single photon. A combination band is when a single photon excites more than one vibration and a hot band is when an already excited vibration is further excited. Overtones and combination bands are generally much less intense than fundamental transitions but an "intensity borrowing" mechanism can add intensity to otherwise weak absorptions. In CO_2 the symmetric stretch should be found at $1337cm^{-1}$ and the bending occurs at $667cm^{-1}$. The first overtone of the bending mode is expected near $2*667 = 1334cm^{-1}$. However, quantum mechanics allow a mixing, called Fermi resonance, between these two modes. The mixing has two effects; the overtone can gain energy from the nearby fundamental and both energy levels are shifted away from the each other. Instead of observing a strong band at $1337cm^{-1}$ and a weak band at $1334cm^{-1}$, two strong bands are observed at $1388cm^{-1}$ and $1286cm^{-1}$.

It is now time to go back to the physical explanation for the Raman effect. If a molecule is placed in an electrical field, ε, a dipole moment, μ_{ind} is induced in the

molecule. The induced dipole is proportional to the field strength, the proportionality constant, α, being called the polarizability of the molecule.

$$\mu_{ind} = \alpha\varepsilon \tag{2.19}$$

All atoms and molecules will have non-zero polarizability even if they have no permanent dipole moment. Consider a light wave whose electrical field oscillates according to the equation

$$\varepsilon = \varepsilon_0 \cos 2\pi\nu t \tag{2.20}$$

The induced dipole moment of a molecule in this oscillating field is obtained from Eq. 2.19 and 2.20.

$$\mu_{ind} = \alpha\varepsilon_0 \cos 2\pi\nu t \tag{2.21}$$

But α is a molecular property and its magnitude will vary as the molecule oscillates.

$$\alpha = \alpha_0 + \Delta\alpha \cos 2\pi\nu_0 t \tag{2.22}$$

α_0 is the equilibrium polarizability, $\Delta\alpha$ is its maximum variation, and ν_0 is the natural vibrational frequency. Putting Eq. 2.21 into Eq. 2.22

$$\begin{aligned}\mu_{ind} &= \left[\alpha_0 + (\Delta\alpha)\cos 2\pi\nu_0 t\right]\left[\varepsilon_0 \cos 2\pi\nu t\right] = \\ &= \alpha_0\varepsilon_0 \cos 2\pi\nu t + 1/2\Delta\alpha\varepsilon_0\left[\cos 2\pi(\nu+\nu_0)t + \cos 2\pi(\nu-\nu_0)t\right]\end{aligned} \tag{2.23}$$

Equation 2.23 predicts that the induced dipole moment will oscillate with components of frequency ν, $\nu+\nu_0$ and $\nu-\nu_0$. The oscillating dipole radiates electromagnetic waves of frequency ν (Rayleigh scattering), $\nu+\nu_0$ (Anti-Stokes) and $\nu-\nu_0$ (Stokes). The selection rule for Raman transition is different from that from IR. A transition is Raman active if the polarizability of the molecule changes during the vibration. The change can be either a change in magnitude or a change of direction of the polarizability. Consider again the three fundamental vibrational modes of the linear CO_2 molecule. We have seen that the

asymmetric stretch and the bending modes are IR active. Now we will see which modes are Raman active. During the symmetric stretch the molecule changes size and therefore it changes the polarizability of the molecule. In the other two modes, α changes with the displacement, ξ, of the atoms, but the change has the same sign for displacements in both directions. Therefore $d\alpha/d\xi$ is zero for small displacements and the modes are Raman inactive. We can see that different modes are IR and Raman active for CO_2. In order to be SFG active the vibration mode must be both IR and Raman active. For CO_2 in gas phase there is no such mode but in other molecules some modes are both IR and Raman active and they are therefore also SFG active.

References

(1) Bass, M.; Franken, P.A.; Hill, A.E.; Peters, C.W.; Weinreich, G. *Phys. Rev. Lett.* **1962** *8*, 18

(2) Bloembergen, N. Nonlinear Optics, Benjamin, New York, **1965**

(3) Hunt, J.H.; Guyotsionnest, P.; Shen, Y.R. Chem. Phys. Lett. **1987**, *133*, 189

(4) Shen, Y.R. "The Principles of Nonlinear Optics" Wiley, New York, **1984**.

(5) Shen, Y. R. *Surf. Sci.* **1994**, *299/300*, 551.

(6) Du, Q.; Superfine, R.; Freysz, E.; Shen, Y.R. *Phys. Rev. Lett.* **1993**, *70*, 2313.

(7) Johal, M.S.; Ward, R.N.; Davies, P.B. *J. Phys. Chem.* **1996**, *100*, 274.

(8) Conboy, J.C.; Messmer, M.C.; Richmond, G.L. *J. Phys. Chem.* **1996**, *100*, 7617.

(9) Shen, R.Y. *Nature* **1989**, *337*, 519.

(10) Buck, M.; Himmelhaus, H. *J. Vac. Sci. Tech. A* **2001**, *19*, 2717.

(11) Hirose, C.; Akamatsu, N.; Domen, K. *Appl. Spect.* **1992**, *46*, 1051.

Chapter 3. Experimental Considerations

3.1 Sum Frequency Generation Setup

SFG experiments are setup with many different designs. However, four groups of components can be distinguished in all setups. First of all, a pulsed laser is needed as the light source. For the experiments reported in this thesis a picosecond Nd:YAG laser was used. For the SFG experiments two different beams are needed, one visible and one tunable IR beam. They are generated in an optic parametric generator/amplifier (OPG/OPA) stage, which is the second part of the setup. This work has been performed on two different OPG/OPAs. The design varies depending on the frequency of IR needed for the experiments, as well as the choice of nonlinear crystals used for the setup, but the function is similar. The third group of components is a series of optics needed to direct the two beams to the sample, to collect the generated signal and send it to the detection system, which is the fourth part.

The laser used for both setups was a Continuum Leopard D-20 laser, which is a picosecond pulsed, modelocked, Nd:YAG laser. The repetition rate was 20 Hz, with a pulse duration of 20ps and an energy output of about 28 mJ/pulse. The explanation for the name Nd:YAG lies in the fact that Nd^{3+} ions replace yttrium ions in the yttrium aluminum garnet ($Y_3Al_5O_{12}$) or YAG. The YAG can be doped with neodymium ions up to a doping level of 1.5% and the main laser transition is at 1064 nm. It is basically a four-level system, schematically shown in figure.3.1. At room temperature almost all the population is in the ground state E_0 before the pumping. The electrons are then pumped to

the level E_3, which can be rather broad in order to increase the pump efficiency. A rapid non-radiative decay follows to the metastable level E_2. If then the decay from E_1 to E_0 is rapid one has an inversion population, which is necessary for laser action, between level E_2 and E_1. The inversion population can be maintained easily with modest pumping. Pulsed operation is obtained with a simple flashlight and reflecting cavity. The optical pulse from the flashtube lasts for a few milliseconds and it takes about a half millisecond to achieve inversion population. Once stimulated emission occurs the upper level is rapidly depopulated, much faster than the pumping re-excitation of electrons, and the laser action stops for a moment until sufficient inversion population can be built up again. Thus the laser has a regular pulsation in the output.

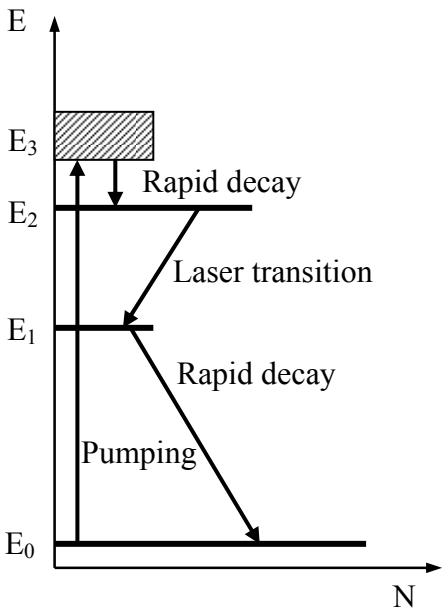

Figure 3.1 Population of the energy levels in a four-level system after pumping.

Q-switching is a technique for obtaining short, intense burst of radiation from the laser. This is achieved by introducing a time-dependent loss in the cavity. The high loss prevents laser action, while energy is being pumped into the excited state of medium. When the cavity loss is suddenly reduced the laser oscillation can begin and all the energy is emitted in a single, large pulse. The switching was achieved by a saturable absorber, which changed from highly absorbing to transparent with the increasing of the irradiance. In a Q-switched pulsed laser a single optical pulse is produced during each pumping pulse but in a mode-locked laser many extremely narrow, equally spaced pulses are produced. A cavity may support many different modes oscillating simultaneously. If the various modes are forced to maintain the same relative phase δ to one another, they are mode locked. This is achieved by modulating the loss in the laser cavity at a certain frequency. The total irradiance is now periodic. To obtain high power and short duration pulses there should be a large number of possible modes. The modulation is accomplished in similar ways as Q-switching. The result was the production of a series of narrow, mode locked pulses contained within a much longer envelope. The peak power within the individual pulses approached 1.5 GW due to the their very short duration.

The OPG/OPA system that was used for the earlier work was a homebuilt system that allowed tuning of the IR from 2-8 μm. The shorter wavelengths, 2-4 μm, were generated in two counter rotating $LiNbO_3$ (LBO) crystals with an approximate output of 300 μJ. To generate longer wavelengths the output from the laser was frequency doubled in a LBO crystal. The resulting 532nm light was used to pump two BBO crystals in an OPG/OPA stage. The idler from this stage was difference frequency mixed with the 1064

in a $AgGeS_2$ crystal to produce wavelengths from 4 to 8 μm with an energy output of 150 μJ/pulse.

The second OPG/OPA setup, which was primarily used in this work and therefore will be described in more detail, has two optical parametric systems both put together and marketed by LaserVision. The fundamental output from the Nd:YAG laser was used to pump both systems. One third of the energy was directed to the optical parametric system designed to create a tunable visible source. There, second and third harmonics of the fundamental 1064nm was generated in two KTP crystals. The generated 355nm light pumped two counter rotating BBO crystals in an OPG/OPA stage. The output form this stage was tunable between 400nm and 700nm. The wavelength of the visible light in the experiments reported in this thesis was held constant at 532nm. The second part of the output from the laser was directed to the optical parametric system designated to generate a tunable IR source. A schematic representation of the parametric converter is shown in figure3.2. Entering the system laser light was divided into two beams by a beam splitter. One beam was frequency-doubled in a KTA crystal to provide the 532 nm pump light for the first OPG/OPA stage. The other part of the beam was sent through a delay before it was recombined with the idler output from the first stage and directed into the second OPA stage. A variable attenuator placed in the second 1064 line was used to correct the polarization and adjust the pump energy delivered to the 1064 nm OPA. A half-wave plate in a rotational stage before the harmonic generator in the 532 line permitted the intensity to be continuously varied. Following the doubling crystal was a 1064 nm high reflecting mirror in order to separate the 1064 nm light from the 532 nm, which is the OPG/OPA pump. When the beam reaches the KTP crystals a fairly broad OPG pulse was

generated. The generated signal reentered the crystal from the other direction together with the residual 532 nm pump beam for amplification. In this way only the central portion of the pulse from the first pass was amplified. Following the 532 nm OPG/OPA, two dichroic mirrors removed the residual 532 pump and separated the signal and idler waves. The idler wave (tunable from 710 to 860 nm) passed through a variable half-wave plate and two beam steering mirrors before being combined with the 1064 nm beam for difference frequency mixing (DFM). Following the 1064 nm OPA was first a dichroic mirror for removing the residual 1064 nm pump then a rotatable stack of plates polarizer to eliminate one of the other of the oppositely polarized signal and idler waves from the infrared output. In both the 532 nm and 1064 nm OPA stages, two crystals of equal length were used and counter-rotated to compensate for beam displacement.

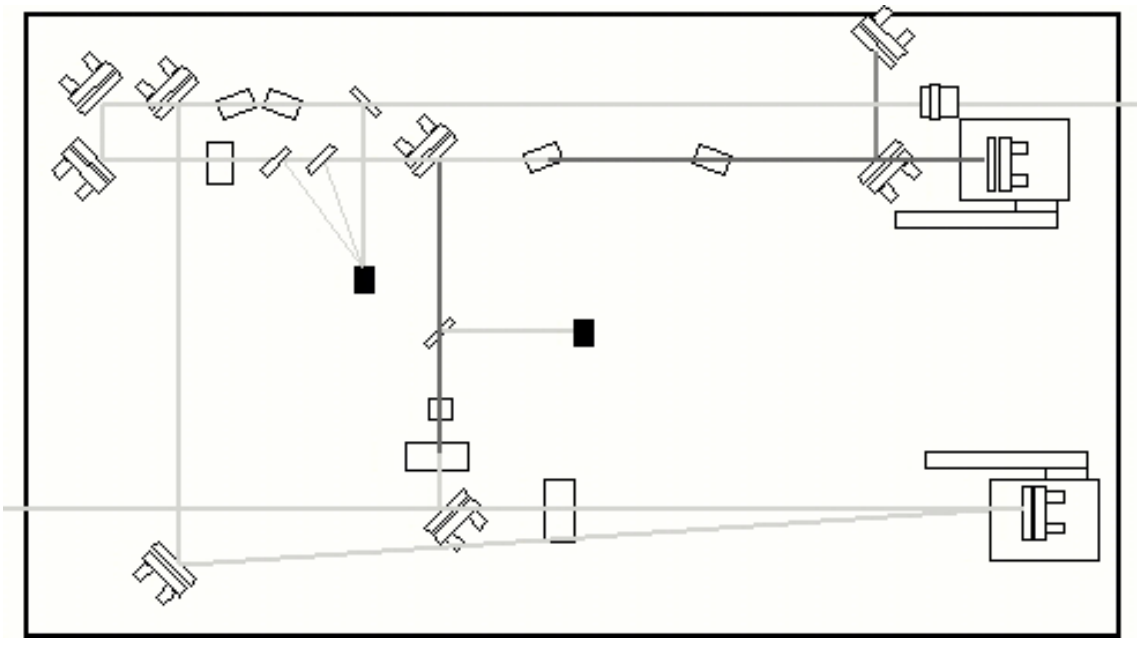

Figure 3.2. Optical layout for the IR OPG/OPA system.

To achieve phasematching for the desired conversion process the parametric converter uses angle tuning. By rotating the crystals in the extraordinary plane with respect to the incoming beam, the refractive index for light polarized in this plane is changed. The rotational plane, parallel to the optical bench, contains the optic axis of the crystal. Rays parallel to it are called extraordinary beams or e-beams and light polarized perpendicular to this plane is termed ordinary beams, o-beams. When the crystal is rotated the refractive index for e-polarized waves varies but the index for the o-polarized waves remain unchanged. Since the rotational plane is parallel to the bench all e-waves are polarized horizontally while all o-rays are vertically polarized. The polarization of the three waves involved in the conversion process is determined by phasematching type in use. The first and second stage all use type II, or eoo, phasematching. eoo means that the signal is an extraordinary wave while the idler and the pump beams both are ordinary waves. In this configuration it correspond to a vertically polarized output. A LabVIEW program was written to control the tunable visible and infrared sources. In the program each individual motor could be controlled and tuned to the positions corresponding to the desired wavelength of the output. The program also collected and charted the data from the signal detection system.

From the OPG/OPAs there are two beams coming out, the 532nm and the tunable IR. Due to adsorption of the IR in the atmosphere the path length for the IR beam was minimized. The light from the OPG/OPA is vertically polarized coming out from the box and with a vertical configuration of the sample this correspond to an s-polarized beam. On metal only p polarized light gives a signal due to selection rules discussed earlier. Therefore, the polarization needed to be changed, which was achieved by two sets of

mirrors. Two lenses are added in the beam line in order to focus the light to a desired spot size on the sample. The path length of the visible beam is not limited by adsorption. Instead the length has to be carefully adjusted so the 532nm pulse arrives at the sample at the same time as the visible. This is done in a time delay stage made of two mirrors mounted on a translation stage. Added in the line is a telescope, consisting of a positive and a negative lens, which makes it possible to change the size of the beam. A half-waveplate followed by a polarizer change the polarization of the light to either s or p-polarized light.

Coming off the surface are the generated sum frequency light as well as the reflected light of the IR and visible. A mirror is placed in the SFG beam line sufficiently far away from the sample in order to spatially separate the SFG signal and the 532 light. The mirror sends the light into the detection line, which has two filters to separate the residual 532nm light from the SFG light. A polarizer makes it possible to measure different polarizations. A focusing lens is inserted in the line as well to collect the sum frequency light and direct it into the monochromator. The monochromator is used to separate the desired wavelength and to send it to the photomultiplier tube (PMT). This is accomplished by a grating inside the monochromator. The light collection, diffraction and focusing to the exit are all done by this grating. To control the bandpass and the amount of light coming in the monochromator slits were placed in the entrance and the exit. During a scan the monochromator was adjusted automatically by a motor control. After the light has passed the monochromator it was directed to the photo multiplier tube. The PMT converts the light to a current that is the output signal from the spectrometer. It consists of a photocathode followed by focusing electrodes, an electron multiplier and an

electron collector in a vacuum tube. When the light hits the photocathode, electrons are emitted from the surface. The electrons are then directed towards the electron multiplier by the focusing electrode. When the electron hits the electron multiplier secondary electrons are emitted from the surface. These electrons are then accelerated to the next dynode where they create a cascade of electrons. Finally the multiplied electrons are collected by the anode and generate the output signal.

The signal from the PMT went through a gated integrator and boxcar averager. It is designed to recover fast repetitive analog signals in the picosecond region. A time gate with a 10ns width was generated and timed by a set delay from an internal or external trigger. The gated integrator amplifies and integrates the signal that is present during the time the gate is open, ignoring noise and interference that may be present at other times. Boxcar averaging refers to the practice of averaging the output of the gated integrator over many shots of the experiment. Averaging N shots will improve the signal to noise ratio by a factor of the square root of N. A computer interface transfers the signal to the computer where the data is collected and treated in a LabVIEW program.

3.2 Ultra High Vacuum system - high pressure reactor

The experiments were carried out in three different vacuum chambers. The chambers were equipped with similar instruments and therefore only one of them is described in detail in this chapter. The specifics of the other vacuum systems are reported in subsequent chapters.

The chamber where most experiments, reported in this thesis, were carried out was a combined Ultrahigh Vacuum/High-Pressure reaction chamber, which was designed and built to allow studies of catalytic reactions under high pressure. It was designed as a two-level system; consisting of an ultrahigh vacuum, surface analysis chamber on top and a high-pressure reaction cell compatible with UHV and SFG mounted on the bottom, see figure 3.3. The base pressure in the UHV chamber was $5x10^{-10}$ Torr, which was achieved by a turbomolecular pump and an ion-pump. The pressure in the vacuum chamber could be maintained while the reaction cell was pressurized to 10 atm. The reaction cell, with a total volume of 170 cm^{-3}, was attached below the main UHV chamber. By lowering the sample holder into the cell a knife-edge was pushed against a gasket and when applying pressure from a hydraulic pump onto the sample holder and gasket, a seal was made between the reaction cell and the UHV chamber. To withstand the applied pressure from the hydraulics the sample holder was constructed with a hollow stainless steal cylinder. A rotatable flange with four feedthroughs made up the interface between the outer atmosphere and the vacuum. Two of those feedthroughs were made of hollow copper tubes and provided electrical heating of the sample and cooling by flow of liquid nitrogen. The other two connections were made to accommodate a K type thermocouple. The hollow steel cylinder was welded to the rotatable flange and provided structural support for the sample holder. When pressed against the gasket the bottom edge of the cylinder made a seal between the reaction cell and the vacuum chamber. To minimize the volume of the reaction cell an additional flange was welded at the bottom of the steel cylinder. The four feedthroughs continued through this flange and the sample was mounted at the end of them. Using the hydraulic pump the sample holder could be raised

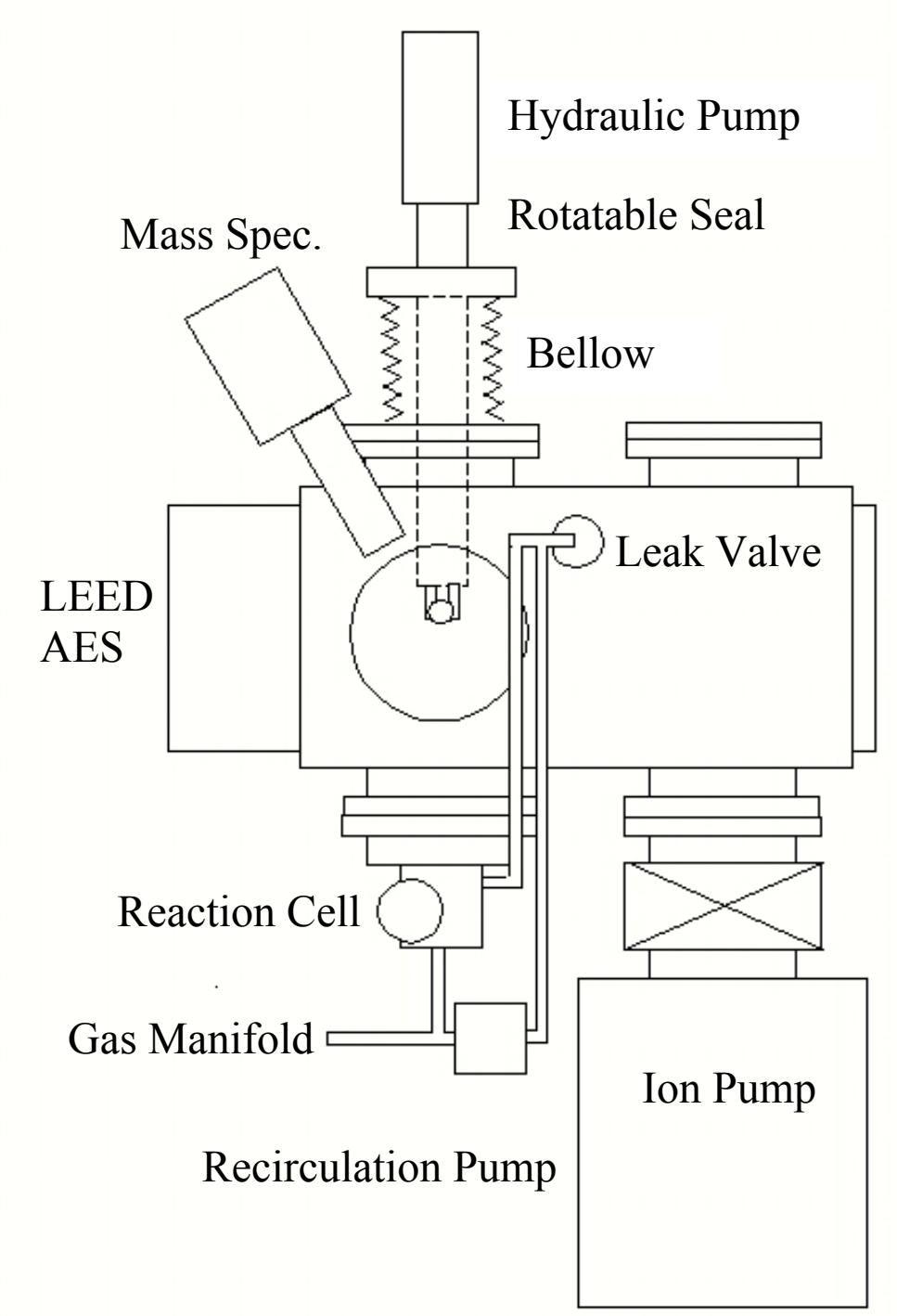

Figure 3.3. Schematics of the integrated ultra high vacuum / high pressure reaction chamber.

and lowered and the sample was moved between the reaction cell and vacuum chamber under ultrahigh vacuum conditions. The system allowed studies of adsorbates from a fraction of a monolayer obtained at UHV to high coverages obtained at atmospheric pressure. For UHV studies the pressure was regulated precisely by a leak valve and measured by an ion gauge in the UHV chamber. High pressure gases were introduced directly from a manifold to the reaction cell where the pressure was monitored by a Baratron gauge. Through a recirculation loop, which was attached to the reaction cell and to a leak valve on the main UHV chamber, the gas composition under high-pressure catalytic conditions could be monitored by a residual gas analyzer. The system was further equipped with a retarding field analyzer, RFA, for Auger electron spectroscopy and LEED analysis, allowing characterization of composition and structure of the surface. The sample was mounted on the sample holder where it could be resistively heated to 1100K or cooled by a flow of liquid nitrogen down to 170K.

For the SFG experiments the reaction cell was equipped with two CaF_2 windows to allow the IR light to reach the sample. The material of the windows and their integration in the flanges were the limiting factor of the pressure in the reaction cell. At high pressures the attenuation of the IR light before it hits the sample becomes more sever. Therefore, the path length from the window to the sample minimized at approximately 4 cm. To normalize for the gas phase adsorption that did occur in the reaction cell the IR power was monitored before and after the reaction cell. The IR power at the sample surface could thereafter be calculated and the SFG intensity was calibrated by the IR power.

Chapter 4. High Pressure Ammonia Adsorption and Dissociation

4.1. Introduction

Iron has been used as the key catalyst for producing ammonia from nitrogen and hydrogen. Consequently, the reaction of ammonia synthesis on iron catalysts has been extensively studied since its discovery in the early 20th century and it has developed into one of the classical heterogeneous catalytic processes. [1] The industrial reaction typically requires high temperatures (300°C to 500°C) and high pressures (tens of atmospheres or higher). Even though this reaction has been industrialized for nearly a century, the intriguing role of iron surfaces has been the focus of decades of studies, to help uncover some of the basic principles of heterogeneous catalysis. Most of the reported fundamental surface science studies are under experimental conditions (high vacuum and low temperatures) far away from industrial conditions, and thus the importance of the information obtained to catalytic ammonia synthesis could be questioned. One of the difficulties of *in situ* studies is that there has been a lack of instrumentation that could enable characterization of catalyst surfaces under the reaction conditions. The application of SFG vibrational spectroscopy to surface chemistry studies has been explored as one of the possible approaches to tackle the obstacles for *in situ* studies of catalyst surfaces under various conditions. [2,3] It should be noted that no SFG studies have been reported on clean iron or iron oxide surfaces so far. Given the active role of iron and iron oxides in heterogeneous catalysis, such effort would be of genuine interest.

Ammonia synthesis, as well as its dissociation process, on iron and other metal surfaces has been pursued for several decades by various surface analysis techniques. Most studies have been performed on high surface area iron catalysts or on single crystals as model catalysts, where for example elementary reaction steps, surface structure, the role of promoters and adsorption behaviors have been investigated. [4] The iron surface with the highest turnover rate was found to be the Fe(111) crystal face. [5] The focus of this study has been on the ammonia adsorption and dissociation on Fe(111) at high pressure (200 Torr). A newly designed integrated UHV-High Pressure system with capabilities for *in situ* SFG was build for the purpose of studying high pressure catalytic processes and in particular ammonia synthesis. The system has a reaction cell that can be pressurized to several atmospheres to more closely mimic the industrial process. The reaction cell is connected to an ultra high vacuum chamber, which allows preparation and characterization of the surface with standard surface science techniques, including ion bombardment, Auger Electron Spectroscopy (AES), Low Energy Electron Diffraction (LEED), and mass spectrometry.

In the present work, adsorption of ammonia has been performed on two surfaces, clean Fe(111) and Fe(111) pretreated with oxygen. Ammonia dissociation intermediates, NH and NH_2, were detected on both surfaces under high pressure of ammonia. Coadsorption of oxygen and ammonia is discussed, and in particular its influence on the SFG spectral features related to the interference between the resonant and non-resonant second order non-linear susceptibility. A weak resonant signal from the NH stretch, in addition to the large non-resonant signal from iron made extensive averaging necessary to obtain a good signal to noise ratio in the SFG spectra.

2. Experimental Section

The UHV / high pressure reaction cell used in this experiment is described in the previous chapter. The Fe(111) single crystal was cut, oriented and polished by normal procedures. Prior to mounting, the Fe(111) crystal was heated to 800°C for several days in flow of hydrogen to remove sulfur impurities. At this temperature the diffusion rate of sulfur is high enough to allow significant amounts of sulfur to segregate to the surface where it is removed by reaction with hydrogen. Thereafter, the Fe(111) crystal was put into the UHV chamber where it was further cleaned by repeated cycles of Ar sputtering at 500°C to remove additional sulfur. Besides sulfur, carbon was the main impurity. Both impurities can be seen by AES in figure 4.1. It was found that the most efficient way to remove carbon impurities was to introduce $1x10^{-7}$ Torr O_2 while sputtering at $3x10^{-5}$ Torr Ar at 500°C, followed by sputtering in pure Ar at room temperature. Between sputtering cycles the sample was briefly annealed to 600°C. This process finally resulted in a clean iron surface with concentrations of impurities below the detection level of AES as seen in figure 4.1. Once a clean iron surface had been obtained only a few sputtering cycles were needed to remove contaminants between each experiment. After annealing of the clean surface the crystal structure was checked with LEED and a hexagonal diffraction pattern, shown in figure 4.2, corresponding to the Fe(111) surface was observed.

The details of the SFG setup have been reported in earlier chapters. In this experiment the visible wavelength was 532 nm. Both IR and visible beams were p-

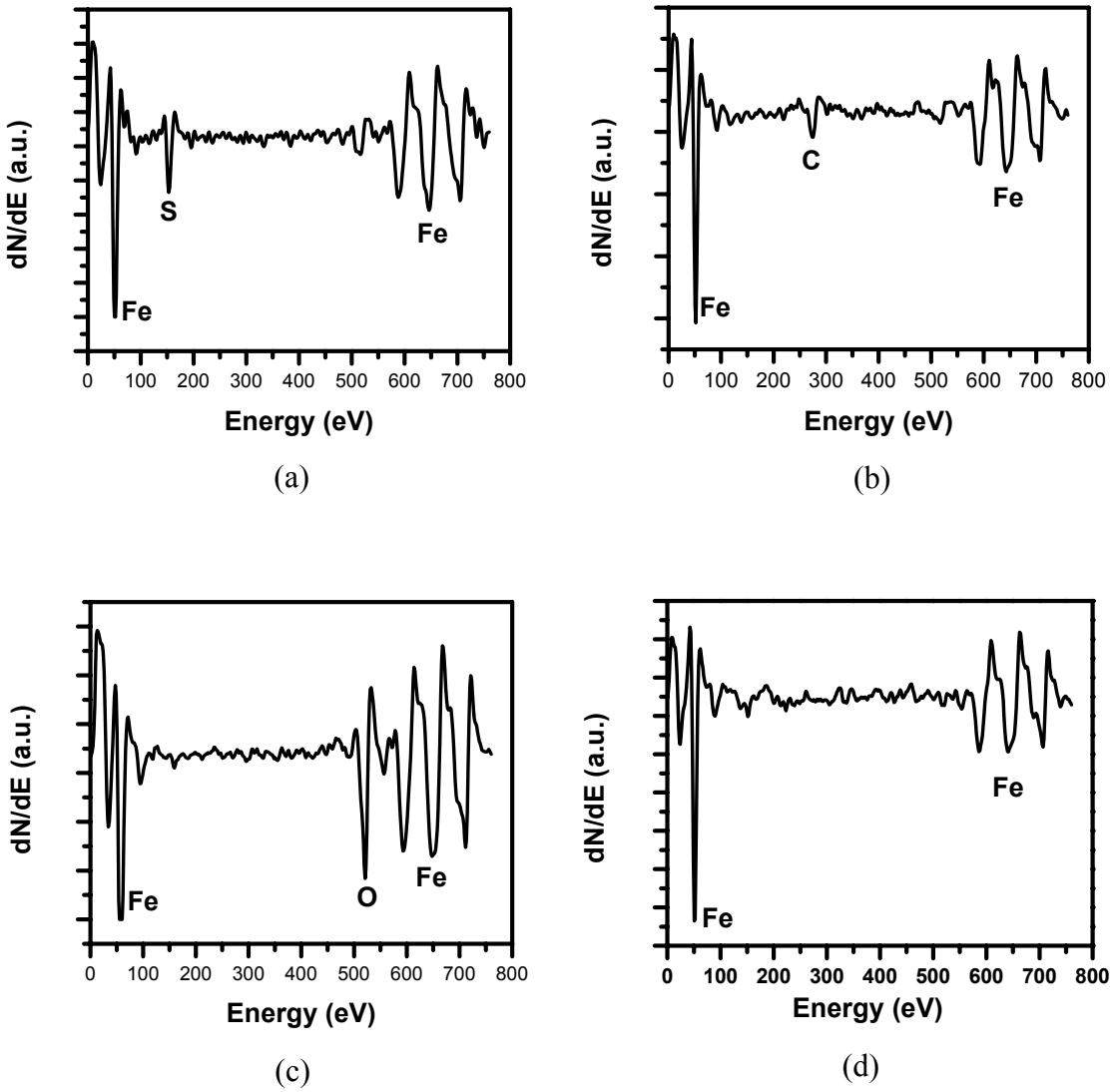

Figure 4.1. Auger electron spectra of clean and contaminated Fe(111) surfaces. (a) The peaks correspond to iron (47, 600, 650, and 700 eV) and with two of its impurities, sulfur and oxygen. (b) Prolonged heating in hydrogen furnace at 800°C removed sulfur while carbon built up on the surface. (c) Sputtering at 500°C with an argon and oxygen mixture resulted in a removal of carbon and an oxidation of the iron. (d) After additional sputtering with pure argon at room temperature a clean Fe(111) surface was obtained.

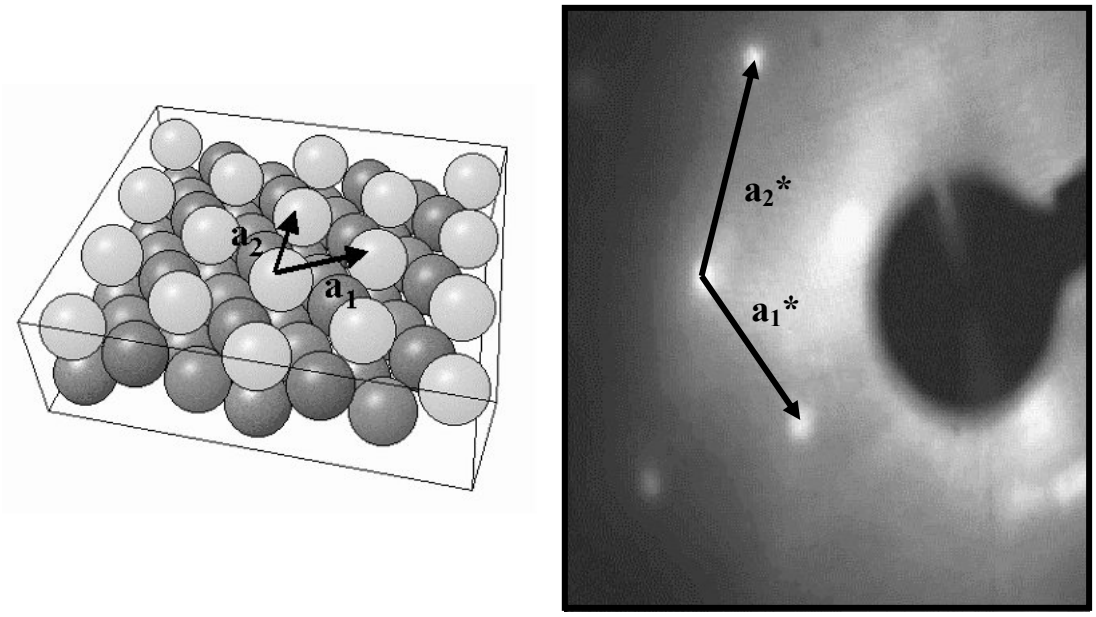

(a) (b)

Figure 4.2. (a) Crystal structure of Fe(111) (b) Corresponding LEED pattern of the Fe(111) surface.

polarized and they were overlapped spatially and temporarily on a Fe(111) crystal. The incident angles of the visible and IR beams were 53° and 62° with respect to the surface normal. The energies of the incident beams were limited to 200 μJ per pulse. To control if the adsorption and dissociation of ammonia is influenced by laser power, both IR and visible beam energies were lowered independently down to 50 μJ. No changes in the spectral features could be seen which indicates that the laser beam does not interfere with the adsorbates. However, one of the main concerns for the study of ammonia dissociation on iron was the weak signal of the NH stretch and the large non-resonant SFG signal of iron. Due to the weak resonant signal of ammonia dissociation products the spectra are

presented with an average of 2000 to 5000 data points per frequency. The experimental data are fitted to Eq. 4.1, described in chapter 2, using a least squares method, to extract the values of parameters, such as peak position, peak width, amplitude, phase and non-resonant background.

$$I(\omega_{sum}) \propto \left| \chi_{NR} + \sum_q \frac{A_q e^{i\theta_q}}{\omega_{IR} - \omega_q + i\Gamma_q} \right|^2 \qquad (4.1)$$

4.3. Results

High pressure (200 Torr) ammonia adsorption on clean Fe(111)

A set of spectra where 200 Torr ammonia have been adsorbed under various conditions is shown in figure 4.3. In the first spectrum, figure 4.3(a), 200 Torr ammonia have been adsorbed on the Fe(111) surface and it resulted in a SFG spectrum with two prominent peaks. After fitting of the experimental data to Eq. 4.1 the peak positions were determined to 3232 cm^{-1} and 3320 cm^{-1}. The peaks are shifted from their apparent peak positions due to the interference between the resonant and non-resonant parts of the second order non-linear susceptibility. The observed peaks are assigned to NH stretch and NH_2 symmetric stretch, respectively. Ammonia adsorption has previously been studied by IR adsorption spectroscopy on powdered iron samples. [6] Peak positions observed in this study correspond well with reported values in the literature. The NH_2 asymmetric stretch is expected to be around 3400 cm^{-1} but no such feature could be seen when adsorbing 200 Torr ammonia on clean Fe(111). There is no evidence of molecular

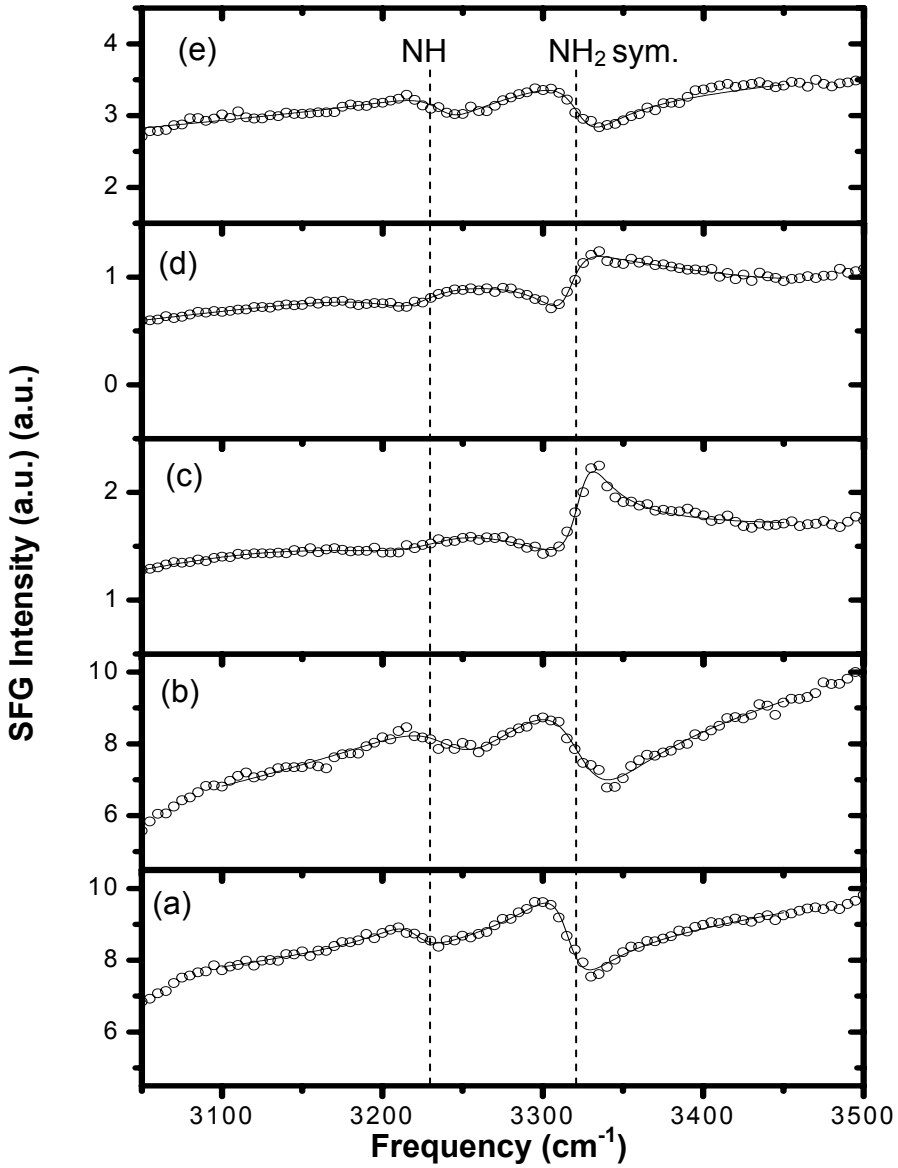

Figure 4.3. SFG spectra of ammonia on Fe(111) and on pre-oxidized Fe(111). Intensities are shown using the same scale for easy comparison. Experimental data are plotted with circles and fitted curves are shown with solid lines. (a) 200 Torr NH_3 on Fe(111), (b) 200 Torr NH_3 on Fe(111) pretreated with 10^{-5} Torr of oxygen, (c) 200 Torr NH_3 coadsorbed with 0.5 Torr of oxygen on Fe(111), (d) 200 Torr NH_3 coadsorbed with 0.5 Torr of oxygen on Fe(111) pretreated with 10^{-5} Torr of oxygen, (e) 200 Torr NH_3 coadsorbed with 0.5 Torr of oxygen on Fe(111) after heating the surface to 150°C for 20 minutes and then cooled down to room temperature.

ammonia on the surface, which could be explained by the rapid ammonia dissociation on clean Fe(111) surface at room temperature. [7] Calculations show that the surface is mostly covered by atomic nitrogen and hydrogen under ammonia synthesis conditions. [8] Only about one to two percent of the sites are covered by intermediates such as NH and NH_2. Although we have performed our experiment under different conditions we believe that the surface is mostly covered by atomic nitrogen and hydrogen. Atomic nitrogen and hydrogen bonded to the surface have vibrational frequencies, 1100 - 500 cm^{-1} for atomic nitrogen depending on bonding geometry, and 1950 cm^{-1} for atomic hydrogen, [9] which are beyond the available frequency range with our SFG setup. Only a small amount of NH and NH_2 intermediates are present on the surface, which make them hard to detect with SFG since minimum coverage for detection is generally around a few percent of a monolayer, depending on the adsorbed species. Another factor that could make the intermediates difficult to detect with SFG is if there is poor, or lack of proper orientation on the surface. Ammonia is adsorbed with the nitrogen towards the iron surface [10] but the molecule could be tilted from the surface normal. To the best of our knowledge there are no reports on the tilt angle of ammonia or its dissociation products on iron. However, a tilt angle up to 40° have been reported for ammonia on the ZnO(1010) surface. [11] Such a tilt angle would reduce the signal intensity in SFG, since it is most sensitive to dipoles perpendicular to the metal substrate.

High Pressure (200 Torr) ammonia adsorption on preoxidized Fe(111)

A near identical SFG spectrum, to the one where 200 Torr ammonia were adsorbed on clean Fe(111), has been recorded on a preoxidized Fe(111) surface as shown

in figure 4.3(b). In this case the Fe(111) surface was exposed to $1x10^{-5}$ Torr of oxygen at room temperature for 20 minutes. Before the introduction of 200 Torr of ammonia the oxygen was pumped out and the surface composition was checked with Auger electron spectroscopy. The SFG spectrum, was fitted to Eq. 4.1 and it shows two peaks at 3241 cm^{-1} and 3326 cm^{-1}, which are attributed to NH and NH_2 symmetric stretches. The peaks are blue-shifted by less than 10 cm^{-1} compared to figure 4.3(a). Again, no peaks due to ammonia were detected. The detection of dissociation intermediates shows that the ammonia at 200 Torr were adsorbed and underwent dissociation on the oxidized Fe(111).

High Pressure ammonia/oxygen coadsorption on Fe(111)

When introducing 200 Torr of ammonia together with 0.5 Torr oxygen on the clean Fe(111) surface the spectrum is different from the previous two cases, see curve (c) in figure 4.3. There are two major differences, the overall magnitude of the non-resonant signal is lowered by introduction of additional oxygen and the spectral features are changed. If curve (a) and (c) are overlapped it can be seen that the peaks in curve (a) are changed into minima in curve (c). At the same time, the minima in curve (a) are changed into peaks for curve (c). Fitting the data shows that the peak positions (3236 and 3324 cm^{-1}) remained close to the previous values but the phases were changed by approximately 180º when the surface was exposed to the additional oxygen. See table 4.1 for a list of the fitting parameters. The peak positions at 3236 cm^{-1} and 3324 cm^{-1} were assigned to NH stretch and NH_2 symmetric stretch, respectively. There is no indication of the presence of molecular ammonia.

Parameters	Fe NH_3	FeO_x NH_3	Fe NH_3/O_2	FeO_x NH_3/O_2	Fe NH_3/O_2 After heating
Peak 1 (cm^{-1})	3232	3241	3236	3229	3237
Phase 1 (deg.)	168	209	35	52	219
Peak 2 (cm^{-1})	3320	3326	3324	3318	3323
Phase 2 (deg.)	188	195	10	-27	205

Table 4.1. Fitting parameters for the experimental data shown in Fig. 2. Presented here are the peak positions and the corresponding phases. Uncertainties for peak positions are ± 2 cm^{-1} and for the relative phase ± 20°. The substrates are either clean Fe(111) or Fe(111) pre-oxidized with 10^{-5} Torr of O_2. Adsorbed gases are 200 Torr of NH_3 or 200 Torr of NH_3 coadsorbed with 0.5 Torr O_2.

When oxygen is introduced together with ammonia there will be a competitive adsorption. The fact that oxygen has about one order of magnitude higher adsorption energy than ammonia[1], which has an adsorption energy of 10-12 kcal/mol [10], means that oxygen adsorption will dominate until the iron surface is fully covered by an oxide layer. The ammonia will then be adsorbed on an essentially oxidized Fe(111) surface. This should be similar to the case of ammonia adsorption on the pre-oxidized Fe(111) in figure 4.3(b). Yet, we see a clear difference between the spectra (b) and (c), which tells us that presence of gas phase molecular oxygen pressure plays an important role. Figure 4.3(d) show the case where 200 Torr of ammonia were coadsorbed with 0.5 Torr of oxygen on a Fe(111) surface pre-oxidized with 10^{-5} Torr of oxygen. No differences to the

coadsorption on clean Fe(111) were found, which confirms that during coadsorption on clean Fe(111) the surface was initially oxidized.

To further explore the coadsorption of oxygen, the Fe(111) was heated up to 150°C for 20 minutes in the presence of 200 Torr ammonia and 0.5 Torr of oxygen. The sample was then cooled down to room temperature before a new SFG spectrum was recorded, see figure 4.3(e). After heating, the spectral features were again reversed and the peaks were determined to 3237 cm^{-1} and 3323 cm^{-1} corresponding to NH and NH_2 symmetric stretch, respectively. The relative phase was switched by nearly 180º as seen in table 4.1.

Pressure effect on ammonia/oxygen coadsorption

To evaluate the effect of pressure on ammonia coadsorption with oxygen, a series of spectra has been recorded at pressures ranging from 10^{-5} Torr to 600 Torr of ammonia. In all cases ammonia have been coadsorbed with oxygen. At 10^{-5} Torr of ammonia, 10^{-5} Torr of oxygen were introduced together with the ammonia. For higher pressures, ammonia was coadsorbed with 0.5 Torr of oxygen. At 10^{-5} Torr no vibrational features could be detected (see figure 4.4). By increasing the pressure to 20 Torr, vibrational features due to ammonia adsorption were visible. Fitting the curve to Eq. 4.1 gives us two peaks centered at 3235 $cm^{-1}$and 3325 cm^{-1}. They are attributed to NH stretch and NH_2 symmetric stretches, respectively. By increasing the pressure to 200 Torr the peaks become more pronounced. Further increase in pressure to 600 Torr does not significantly alter the spectrum. After pumping out the ammonia there are no observable peaks in the spectrum.

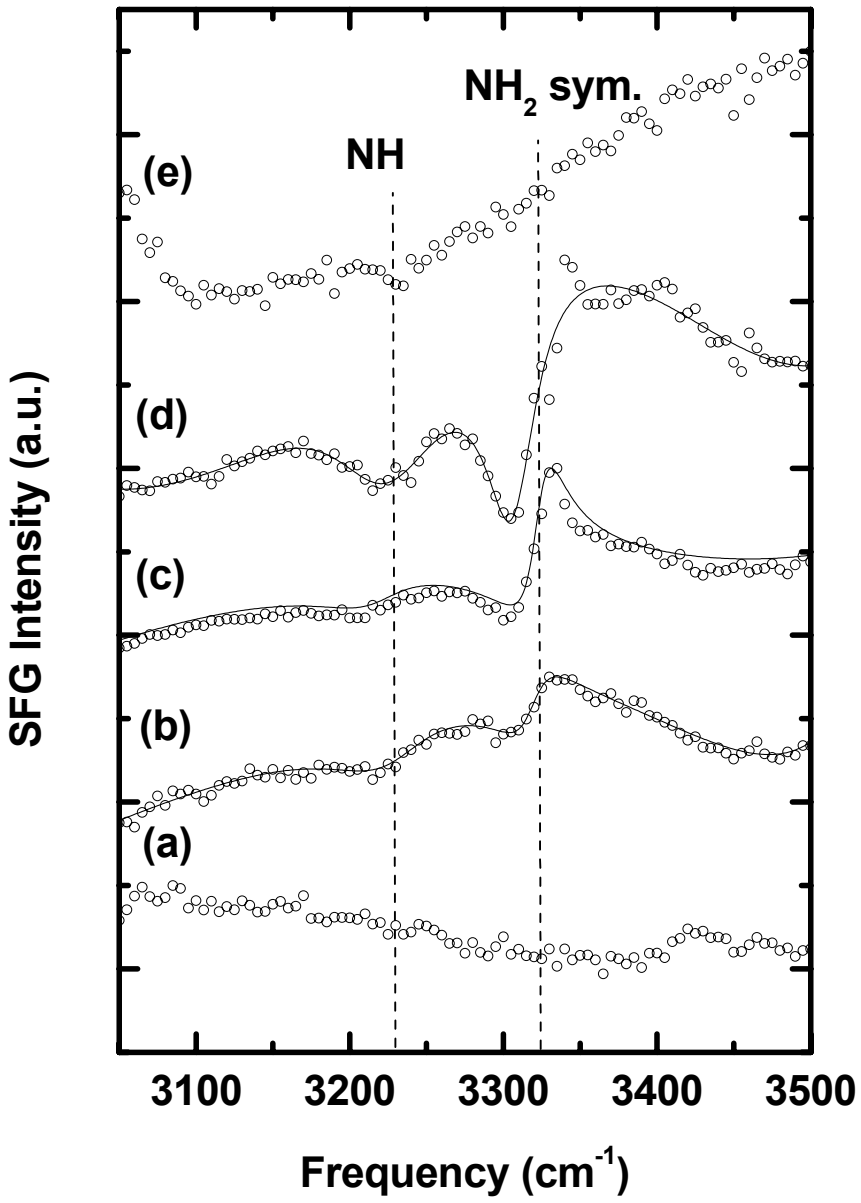

Figure 4.4. SFG spectra of ammonia coadsorbed with oxygen on pre oxidized Fe(111). Experimental data are plotted with circles and fitted curves are shown with solid lines. (a) 10^{-5} Torr of ammonia and 10^{-5} Torr of oxygen, (b) 20 Torr ammonia and 0.5 Torr oxygen, (c) 200 Torr ammonia and 0.5 Torr oxygen, (d) 600 Torr ammonia and 0.5 Torr oxygen, (e) SFG spectrum after pumping out of the ammonia and oxygen.

4.4. Discussion

When ammonia is adsorbed on clean or preoxidized Fe(111) surfaces NH_2 and NH species were detectable in a broad range of experimental conditions. In contrast, we were not able to detect molecular ammonia at room temperature in our studied pressure range (10^{-5} - 600 Torr). In this study we have been concentrating on high ammonia pressure and high temperature experiments (room temperature or above).

When pure ammonia is adsorbed on clean Fe(111) two peaks with asymmetric profiles can be seen with at 3232 cm^{-1} and 3320 cm^{-1}. Pre-oxidizing the Fe(111) in $1x10^{-5}$ Torr oxygen for 20 minutes does not greatly change the peak positions of the NH and NH_2 surface species. Several conclusions can be drawn from this. First ammonia can decomposes on the pre-oxidized as well as the clean Fe(111) surface. There is a possibility that the oxide is reduced by the high pressure ammonia and exposed iron sites are responsible for the dissociation. However, the oxygen coverage before and after ammonia adsorption was measured by Auger electron spectroscopy and no reduction of the oxygen peak could be seen. The second conclusion is that the dissociation products are loosely bound to the surface and that the bond strength to the surface does not change appreciably whether adsorbing on the clean or preoxidized Fe(111). Lastly, the relative phase between the resonant and non-resonant part does not change by pre-oxidizing the surface.

The largest changes in the spectral features was seen when 0.5 Torr of oxygen was coadsorbed with ammonia and after heating of the surface. Analysis of the data shows a phase shift of close to 180° between the resonant and non-resonant part of the

SFG signal when 0.5 Torr oxygen was present. Upon heating the surface to 150°C the spectral features are reversed and the relative phase were again changed by 180°. The change in spectral features are caused by an interference between the resonant and non-resonant second order nonlinear susceptibility, which can cause the SFG spectral profile to be different from those observed in IR spectroscopy. Well defined symmetric peaks can be expected in the SFG spectrum when χ_{NR} is negligibly small and resonances are far apart. However, when $|\chi_{NR}|$ is comparable to, or larger than $|A_q/\Gamma_q|$ spectral profiles can include asymmetric peaks and dips. This is the case when using Fe(111) as a substrate. In order to deduce the parameters characterizing the resonances, Eq. 4.1 is used to fit the observed spectrum.

The relative phase shift could be caused by a shift in phase for either the adsorbates or the substrate, or a combination of both. The phase shift was not observed after pre-oxidizing at $1x10^{-5}$ Torr of oxygen indicating that a higher oxygen pressure is needed to induce the phase shift, either by increasing the oxidation of the iron or by being present as molecular adsorbates on the surface of iron. After heating the surface in the presence of oxygen and ammonia the oxygen coverage of the surface was reduced as seen by AES and the spectral features were again reversed. Oxygen re-adsorption and oxidation of the surface was prevented by higher nitrogen coverage on the surface after the increased dissociation of ammonia at high temperature.

In contrast to the large phase shifts due to oxygen coadsorption there were no significant shift in peak positions, which indicates that the bonding to the surface is the similar in all cases. In a related study of coadsorption between CO and NH_3 on Ru(0001) it was concluded that the adsorption of CO, which is an electron acceptor like oxygen,

did not modify the electronic interaction between the ammonia and the metal. [12] The electron donating character of ammonia was the same whether ammonia bonded directly to the metal alone or in the presence of adsorbed CO.

We have also observed that the pressure is important for the detection of ammonia adsorption by SFG. The SFG signal intensity depends on the number density of adsorbed molecules as well as their molecular orientation. Vibrational features from NH stretches are only visible at higher pressures (above 10^{-5} Torr) as seen in figure 4.4. The reason for the pressure dependence could be that the surface coverage is higher at higher pressures. Increasing coverage may induce ordering on the surface where NH and NH_2 radicals are aligned with their dipoles perpendicular to the surface. To analyze the orientation of the molecules on the surface we need at least one more input and output beam polarization combination. The data presented here are from ppp polarization. Therefore, we can not deduce any orientation of the adsorbates from our experiments. Instead we can only speculate that the higher ammonia pressure increases the surface coverage and causes the molecules to align perpendicular to the surface.

4.5. Conclusions

Sum frequency generation vibrational spectroscopy has been used to study ammonia adsorption and dissociation on Fe(111) and preoxidized Fe(111) under high pressure (200 Torr). Vibrational frequencies for NH and NH_2 have been identified on the clean and pre-oxidized Fe(111). Ammonia molecules have been found to dissociate at room temperature on both clean and preoxidized Fe(111) under high pressure (20 - 600

Torr). Introduction of 0.5 Torr of oxygen changes the interference of the resonant and the non-resonant second order non-linear susceptibility by changing the relative phase. This can be seen as a reversal of the spectral features in the SFG spectra. Heating the surface in presence of high pressure ammonia reduces the oxygen coverage and there is another relative phase change of 180° to restore the initial spectral features.

References:

(1) Somorjai, G.A. Introduction to Surface Science and Catalysis, Wiley, New York, 1994.

(2) Buck, M.; Himmelhaus, H. *J. Vac. Sci. Tech. A* **2001**, *19*, 2717.

(3) Somorjai, G.A.; Rupprechter, G. *J. Phys. Chem. B* **1999**, *103*, 10, 1623.

(4) Ertl, G. *Angew. Chem. Int. Ed.* **1986**, *6*, 558.

（5） Strongin, D. R.; Somorjai, G. A. *J. Catal.* **1988**, *109*, 51.

(6) Nakata, T. *J. Chem. Phys.* **1982**, *76*, 12, 6328.

(7) Shvachko, V. I.; Fogel, Y.M. *Kinet. Katal.* (English Ed.) **1966**, *7*, 635.

(8) Bowker, M.; Parker, I.; Waugh, K.C. *Surf. Sci.* **1988**, *197*, L223.

(9) Zhang, H. B.; Schrader, G. L. *J. Catal*. **1986**, *99*, 461

(10) Grunze, M.; Bozso, F.; Ertl, G.; Weiss, M. *Appl. of Surf. Sci.* **1978**, *1*, 241.

(11) Ozawa, K.; Hasegawa, T.; Edamoto, K.; Takahashi, K. Kamada, M. *J. Phys. Chem. B* **2002**, *166*, 9380.

(12) Rosenzweig, Z.; Asscher M.; Wittenzellner C. Surf. Sci. Lett. **1990**, *240*, L583.

Chapter 5. SFG non-resonant signal intensity of Fe(111)

5.1. Introduction

In heterogeneous catalysis, the surface of the catalyst has been always been the center of research. Some questions that scientist have been trying to answer are: What are the structure, composition and electronic properties of the catalyst during the reaction? [1] To answer these questions there is a need for techniques that are surface sensitive and can probe the surface in the presence of the reactants. Often the surface is well characterized prior to the reaction by various techniques, such as AES, XPS, LEED, etc. However, with adsorption of gases the surface structure might change, as seen in the CO adsorption on Pt(100). [2] In vacuum the Pt(100) reconstructs to pseudo-hexagonal (5x20) structure, which is similar to the (111) surface. When this surface is exposed to CO the surface reconstruction relaxes back to (1x1) structure.

The surface composition of the catalyst changes as well during the reaction. The composition can be measured before and after the reaction as shown in one study of ammonia synthesis on iron surfaces. [3] It was found that the amount of potassium, which is one of the promoters added to the surface, decreased during the reaction. With addition of aluminum a higher concentration of potassium where maintained. Surface nitrogen was detected in all cases after the reaction. However one question remains: is the surface after the reaction representative for the surface conditions during reaction? It would be of great interest to monitor the surface, in situ, during the reaction. One surface sensitive technique that is not limited to studying the surface subsequent to the reaction is second

harmonic generation, SHG. SHG is sensitive to changes in surface electron density induced by adsorption and changes in number density and orientation of adsorbed molecules. [4] SHG has primarily been used to study adsorption processes with only one adsorbed species. However, using phase sensitive detection adsorbate specificity has been obtained and catalytic reactions have been studied. [5] Another technique that has the same intrinsic surface sensitivity is sum frequency generation, SFG. Part of the information obtained in SFG spectroscopy is vibrational spectra of the adsorbates on the surface. This has been the primarily objective to use SFG, however the signal intensity also depends on the non-resonant contribution and the interference between the non-resonant and the resonant term. The magnitude of the non-resonant contribution can change the spectral features as displayed in previous chapter. Recently, there have been studies where the change in non-resonant signal, off any vibrationally resonant frequencies, has been used as a probe of the surface during adsorption. [6] Measuring SFG to obtain information about adsorbates through vibrational spectra as well as probing the surface electronic structure of the surface by following the non-resonant signal utilizes the full capabilities of SFG. In previous chapter the study of adsorption of ammonia on Fe(111) was reported. In this chapter the change in non-resonant signal upon adsorption on Fe(111) is investigated.

It was found that Fe(111) had a large SFG non-resonant signal. In addition, the magnitude of the SFG non-resonant signal was significantly changed by the adsorption of N_2, H_2, O_2 and NH_3, species that are most relevant in ammonia synthesis. The change in non-resonant signal was correlated to the change in work function of Fe(111) upon adsorption.

5.2. Experimental Setup

The ultrahigh vacuum chamber used in this experiment is described in the previous chapters. Details of the of the cleaning procedure of the Fe(111) single crystal can be found in chapter four. Briefly, after the crystal was cut and polished it was heated in a hydrogen furnace to remove sulfur. The cleaning continued in the UHV chamber by repeated sputtering and annealing cycles. Auger electron spectroscopy was used to confirm the cleanliness of the sample surface. After the last annealing the crystal structure was checked with LEED. AES spectra and diffraction pattern of the Fe(111) surface were shown in chapter 4, figure 4.1 and 4.2. Once a clean iron surface had been obtained only a few sputtering cycles were needed to remove contaminants between each experiment.

The details of the SFG setup have been reported in earlier chapters. In this experiment the visible wavelength was 532 nm. Both IR and visible beams were p-polarized and they were overlapped spatially and temporarily on a Fe(111) crystal. The incident angles of the visible and IR beams were 53° and 62° with respect to the surface normal. The energies of the incident beams were adjusted to 200 μJ per pulse, which were below the damage threshold of the surface.

5.3. Results

With the visible beam fixed at 532 nm and the IR beam tuned between 3000 cm^{-1} and 4300 cm^{-1} a large SFG signal has been detected from the clean Fe(111) surface.

Within the mentioned frequency range the non-resonant signal is nearly constant up to 3900 cm^{-1} where after it is enhanced by more than three times. When adsorbing various molecules on the clean iron surface we found that the non-resonant signal intensity changed dramatically. The observed changes depend on the adsorption species, as seen in figure. 5.1 The non-resonant signal of Fe(111) was measured at 3300 cm^{-1} where the intensity of the clean Fe(111) surface was normalized to 1. Oxygen and nitrogen are found to decrease the non-resonant signal, while hydrogen increases the signal intensity. Adsorption of ammonia initially increases the SFG signal followed by a gradual decrease as explained later. Changes in second order non-linear susceptibility upon adsorption have previously been observed with second harmonic generation (SHG). [7] However, SFG probes the vibrational features of the adsorbates as well, which could be advantageous over SHG in many experiments.

The gas that was found to have the largest effect on the non-resonant signal was oxygen. The intensity was instantly lowered to 4 times compared to clean Fe(111) when introducing $1x10^{-5}$ Torr of oxygen. By introducing a lower pressure of oxygen, $1x10^{-7}$ Torr, the SFG intensity decreased to the same level as for 10^{-5} Torr, but the decline could be followed on a timescale of several tens of seconds. The fact that the iron surface would be covered by a monolayer within 10 seconds at 10^{-7} Torr indicates that the decline in SFG signal intensity is governed by some other factors besides adsorption of oxygen. A plausible cause could be the formation of iron oxide that could be slower than adsorption and it would also be dependent on such factors as temperature and partial pressure of oxygen.

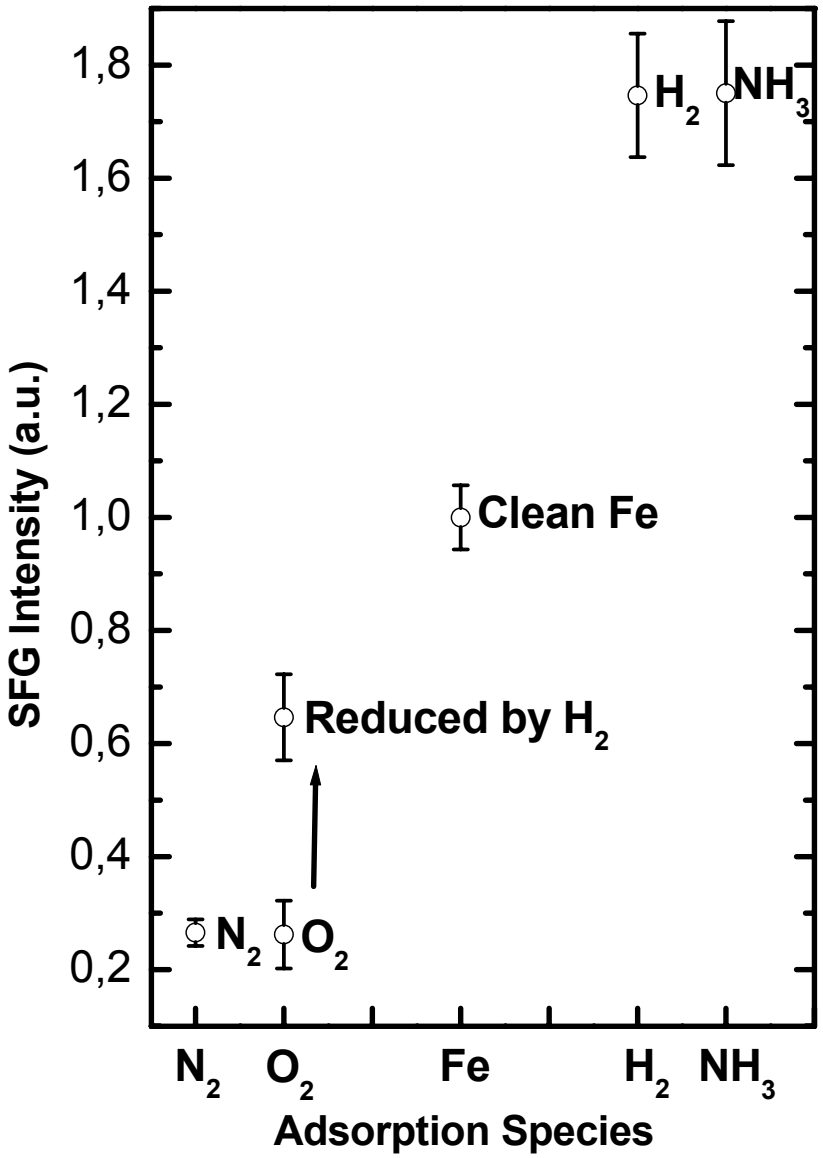

Figure 5.1. SFG background of various adsorbates on Fe(111) measured at 3300 cm^{-1}. The SFG Background intensity of clean Fe(111) is normalized to 1. The intensities are changed upon adsorption of N_2, O_2, H_2 and NH_3. An example of surface reaction monitored by the SFG background is the oxidation of Fe(111) in 10^{-5} Torr of O_2, followed by reduction in 10^{-5} Torr H_2 at 400°C.

No change in intensity has been found when introducing $1x10^{-5}$ Torr of nitrogen at room temperature. This is not surprising since the sticking coefficient of nitrogen is extremely small at room temperature, as low as 10^{-7} on iron. [8] In order to increase the nitrogen coverage the temperature was raised to 500°C while maintaining the nitrogen pressure at $1x10^{-5}$ Torr for prolonged time. Subsequently the nitrogen coverage on the surface was detectable by AES. After cooling down to room temperature the SFG signal had decreased 4 times relative to clean Fe(111). Both oxygen and nitrogen were found to decrease the SFG signal intensity.

In contrast, when $1x10^{-7}$ Torr of hydrogen was introduced the signal increased to 1.7 times that of clean Fe(111). Another case where the intensity was increased is the adsorption of ammonia. The signal was increased by 1.7 times to clean Fe(111) when the reaction cell was pressurized to $1x10^{-7}$ Torr of ammonia. However, ammonia molecules decompose on Fe(111) at room temperature and eventually a nitrogen coverage is built up on the surface. As mentioned before formation of nitride on the surface has an effect of lowering the SFG signal. Over time, as more ammonia decomposed, the surface coverage of nitrogen was increased and the signal intensity dropped below that of clean Fe(111). This is an example of how changes in the non-resonant signal of iron can be used as an indicator of the surface conditions during reaction. As reported above, the formation of oxide on Fe(111) was followed by measuring the SFG non-resonant signal. Under favorable conditions, the kinetics of the oxide formation is slow enough to be monitored by SFG. Another surface reaction that was monitored, was the reduction of iron oxide by heating in hydrogen, see figure 5.1. Introduction of $1x10^{-5}$ Torr of oxygen lowered the SFG signal to 0.25 of that of clean iron. After pumping out the oxygen the

cell was pressurized to $1x10^{-5}$ Torr of hydrogen and heated up to 400°C. As a result the signal intensity was restored close to that of clean Fe(111) indicating that the oxide is reduced by hydrogen. A decrease of the oxygen coverage was also confirmed by AES immediately following the reduction.

As mentioned earlier, clean iron has a large non-resonant background in the studied frequency range (3000 - 4300 cm^{-1}). The maximum amplitude of the signal in this region is comparable to that of gold, which has a high SFG non-resonant background under the same conditions. [9] The lower frequency limit was chosen to include possible NH vibrational modes, while the high frequency was limited by the OPG/OPA. Within the chosen frequency range the SFG signal has a strong dependence on the IR frequency, see figure 5.2. The spectrum can be divided into three parts. In the first range, between 3200 cm^{-1} and 3600 cm^{-1}, the spectrum is relatively featureless. In the center range of the spectrum, around 3600 cm^{-1} to 3900 cm^{-1}, the IR is attenuated by absorption by water in the air before it reaches the reaction cell. Despite normalization of the sum frequency intensity to the IR power at the sample surface there remains a feature in this region. Beginning around 3900 cm^{-1} there is a large increase in the background signal and it is significantly enhanced within 100 cm^{-1}. The abrupt enhancement of the background intensity can not be explained by changes in the IR power. Instead it has to be considered inherent to the iron electronic structure. The same spectrum has been observed for both annealed Fe(111) and on the roughened Fe(111) surface directly after sputtering. The background is therefore not caused by the structure of the crystalline Fe(111) surface. Electron excitations usually require energies of a few eVs, which is above the IR energy (0.39 to 0.53 eV). The resulting energy range, with fixed visible light at 532 nm and

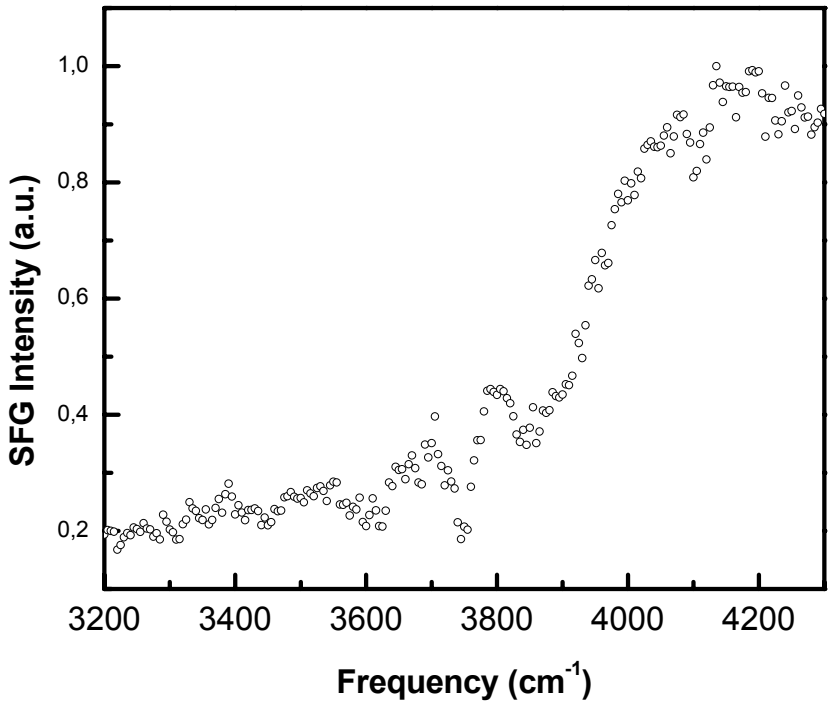

Figure 5.2. Non-Resonant SFG signal from clean Fe(111)

tuning the IR between 3200 and 4300 cm^{-1}, corresponds to 2.73 to 2.87 eV, which would be a suitable range for electronic excitations.

5.4. Discussion

The SFG non-resonant background for metals can in general be related to the electronic structure of the substrate and more specifically the density of states of electrons and the excitations of those electrons. [9] Noble metals, such as gold have completely filled d-band electrons lying below the Fermi level. In the case of gold the d-band is centered 2.58 eV, or 480 nm, below the Fermi level. [10] By tuning the visible input in SFG a large enhancement in the non-resonant signal can be seen in around 480 nm that can be explained by optically excited transitions of electrons between the d- and s-bands. [9] 532 nm light, which has been commonly used in SFG, is close enough in energy to cause electronic transitions. However, by using 1064 nm as the input beam for SFG the background for gold has been substantially reduced. [11] For other transition metals, like Pt, the situation is different and the Fermi level is located inside the d-band. The SFG process can excite electrons from the s- to the d-band, but the s-band is broad and the non-resonant signal in SFG is therefore small and relatively constant in the frequency range used in SFG. For iron, one would have expected a low non-resonant background similar to platinum, but instead signal intensity comparable to gold has been observed. A possible explanation could be associated with the detailed structure of the density of states (DOS) for Fe(111). By tuning the visible light frequency, a larger energy range could probed, which would give a more complete picture of the electronic structure

of Fe(111). However, the focus of this study is not to investigate the surface electronic structure of Fe(111). Instead the dependence of the SFG non-resonant signal is used as a sensitive tool to the changes in the surface electronic density due to chemical interaction with adsorbates.

From the adsorption experiments on Fe(111) it is clear that the information gained by SFG is not limited to the vibrationally resonant signal; changes in the non-resonant signal can also provide useful insight of the surface chemistry. Similar ideas have been reported previously in literature where the non-resonant signal of MgO(001) was monitored during adsorption of formic acid. [6] It was noted that the non-resonant signal intensity decreased upon adsorption of formic acid. Subsequent heating of the surface and desorption of formic acid restored part of the intensity. It was concluded that the non-resonant signal originated from the defect sites and therefore the concentration of these defect sites could be monitored during adsorption and desorption. In this study, the non-resonant signal intensity can both increase and decrease depending on different adsorption species, suggesting there must be some other effects influencing the SFG non-resonant signal intensity.

A possible explanation were given by Guyot-Sionnest et al in a study where the adsorption and desorption of CO on W(110) were investigated. [12] It was shown that there was a correlation between the intensity of the SFG non-resonant signal and the change in work function upon adsorption. The idea of a correlation of the non-resonant signal with work function changes has long been reported in SHG studies. One of the earlier ones discussed the adsorption of O_2, CO, H_2 and NH_3 on Re(0001). [7] It was shown that the SH signal decreased when the surface was covered by electron

withdrawing adsorbates, which increase the work function of the metal, such as O_2 or CO. At saturation coverage of oxygen, the work function was increased by 0.45 eV, and the SH signal showed a fivefold reduction. Upon adsorption of NH_3 the SH signal was increased by 55 times for NH_3 which correlated with a decrease in work function by 2.1 eV.

This study is one of the first SFG studies where changes, both increase and decrease, of the non-resonant signal could be correlated to work function changes of the metal substrate. Oxygen decreased the non-resonant signal by 4 times when adsorbed on the Fe(111) surface. The work function change for this system has previously been shown to increased by 1.1 eV for 2L of oxygen, adsorbed at 77K, on the Fe(111) surface. [13] Nitrogen adsorption also showed a decrease in non-resonant signal, which correlates with a 0.25 eV increase of the work function for Fe(111) upon adsorption of nitrogen. [8] The change depends on coverage for both O_2 and N_2, as well as the heat treatment of the surface in order to obtain nitrogen coverage. In contrast to oxygen and nitrogen, ammonia is an electron donor that give rise to a reduction of the work function, by 2.05 eV, for Fe(111) [14] which agrees with the observed increase of the non-resonant background. Interestingly the initial reduction was followed by a rise of the work function due to ammonia dissociation and the build up of nitrogen coverage on the surface. The final work function was increased by about 0.1 eV compared to the clean Fe(111). This correlates remarkably well with the changes in the non-resonant background, where an initial increase in signal followed by a gradual decrease was observed until the signal stabilized below the signal intensity of clean Fe(111). In the case of hydrogen adsorption the picture is not as clear. The work function has been measured to be between -0.1eV

and 0.3eV depending on the surface structure of iron. [15] Hydrogen adsorption on Fe(111) is reported to give an increase of 0.3 eV. This should lead to a lowering of the non-resonant signal, however, we have observed an increase. Since the work function change is relatively small and can be either positive or negative depending on the surface, a small amount of surface defects could alter the total work function change or the non-resonant signal intensity.

5.5. Conclusions

Fe(111) has a strong non-resonant SFG signal. The change in non-resonant SFG intensity upon tuning is associated with the detailed surface electronic structure of Fe(111). Adsorption on Fe(111) causes a distinct change in the SFG signal and a correlation between the work function change and magnitude of the non-resonant SFG signal is proposed. Knowing the effect on work function upon adsorption, the change of non-resonant SFG signal can be predicted. The change in SFG non-resonant signal can be used to follow surface reactions, including iron oxidation, ammonia dissociation and nitride formation on iron surfaces as well as reduction of iron oxides.

References:

(1) Somorjai, G.A. Introduction to Surface Science and Catalysis, Wiley, New York, **1994**.

(2) Morgan, A.E.; Somorjai, G.A. *Surf. Sci.* 1968, *12*, 405.

(3) Bare, S.R.; Strongin, D.R.; Somorjai, G.A. *J. Phys. Chem.* **1986**, *90*, 4726.

(4) Corn, R.M.; Higgins, D.A. *Chem. Rev.* **1994**, *94*, 107.

(5) Eisert, F.; Rosen, A. *Phys. Rev. B* **1996**, *54*, 14061.

(6) Yamamoto, H.; Watanabe, N.; Wada, A.; Domen, K.; Hirose, C. *J. Chem. Phys.* **1997**, *106*, 4734.

(7) Rosenzweig, Z.; Asscher, M. *Surf. Sci.* **1988**, *204*, L732.

(8) Bozso, F.; Ertl, G.; Grunze, M.; Wiess, M. *J. Catal.* **1977**, *49*, 18.

(9) Dreesen, L.; Humbert, C.; Celebi, M.; Lemaire, J. J.; Mani, A. A.; Thiry, P. A.; Peremans, A. *Appl. Phys. B* **2002**, *74*, 621.

(10) Cooper, B. R.; Ehrenreich, H.; Philipp, H. R. *Phys. Rev. A* **1965**, A494.

(11) Potterton, E. A.; Bain, C. D. *J. of Electroanalytical Chemistry* **1996**, *409*, 109.

(12) Schröder, U.; Guyot-Sionnest, P. *Surf. Sci.* **1998**, *421*, 53.

(13) Borgmann, D.; Kiessling, W.; Stadelmann, M.; Wedler G. *Surf. Sci.* **1991**, *251*, 831.

(14) Grunze, M.; Bozso, F.; Ertl, G.; Weiss, M. *Appl. of Surf. Sci.* **1978**, *1*, 241.

(15) Bozso, F.; Ertl, G.; Grunze, M.; Weiss, M. *Appl. of Surf. Sci.* **1977**, *1*, 103.

Chapter 6. CO Poisoning of catalytic ethylene hydrogenation

6.1. Introduction

Deactivation of catalysts is one of the major concerns in the development of efficient catalysts. Various reactants, intermediates, products or even unexpected foreign atoms and molecules may cover the catalysts' surface during the catalytic reaction. These surface substances could block the catalytic active sites or modify the electronic properties of the catalysts, and as a result, the overall properties of the catalyst can change over time. [1] For example, if one or more of the reaction products are strongly adsorbed on the active sites, it could lead to self-poisoning. Undesired substances from the reaction mixture could adsorb on the surfaces rendering the catalyst inactive. Not all the adsorbed species will deactivate the catalyst. Some of them indeed promote the desired reaction pathways by either reducing the activation energy or selectively blocking the undesired catalytic sites. To engineer better catalysts, it is crucial to understand what the influence is of the coadsorbed species on the catalysts' surfaces and their roles in the catalytic reactions. In the past, most of the mechanistic studies of catalyst poisoning have been focused on using surface techniques, such as low-energy electron diffraction (LEED), Auger electron spectroscopy (AES), electron spectroscopy (UPS, XPS), temperature programmed desorption (TPD), high-resolution electron spectroscopy (HRELS) and infrared reflection spectroscopy (IRS). [2] However, most of these surface techniques are operated under vacuum conditions and little is known about the behavior of the adsorbates in the high-pressure reactions. To fully understand the poisoning

mechanism, it is desirable to monitor these species under reaction conditions. In this chapter, the effect of CO poisoning on ethylene hydrogenation on the Pt(111) surface at 10 Torr of ethylene and 100 Torr of hydrogen is reported.

As an interface-specific vibrational spectroscopic tool, SFG has been used to investigate various surfaces and interfaces including model catalyst surfaces, [3-6] electrode surfaces, [7,8] liquid surfaces, [9-11] and liquid-liquid interfaces. [12] In most cases, it has been shown that the SFG technique is capable of monitoring in situ surface vibrational spectra with sub monolayer sensitivity. To investigate the CO poisoning effect, the vibrational spectra of CO and ethylene coadsorption on the Pt(111) surface were studied. Specifically, the Pt(111) surface was pretreated with a monolayer of ethylene or CO and the surface vibrational spectra were then taken at different CO or ethylene pressures. Previous studies have shown that the adsorbed ethylene molecules form ethylidyne on the Pt(111) surfaces at room temperature and these strongly bonded ethylidyne molecules are believed to be spectators in the ethylene hydrogenation reactions. [13-14] The experimental results indicate that the adsorbed ethylidyne molecules could be partially displaced by introducing high pressure CO. However, when the surface was covered with a monolayer of CO, ethylene molecules could not effectively adsorb on the Pt(111) surface even in the presence of high pressure ethylene. Therefore, CO could block the active site and inhibit the catalytic activity. In fact, in subsequent ethylene hydrogenation studies, it was found that the presence of CO poisons the catalytic reaction and no reaction was observed at temperatures below the CO desorption temperature. The measured apparent activation energy for the ethylene

hydrogenation reaction in the presence of 3 Torr of CO was about 20 kcal/mol, which was much higher than 10 kcal/mol measured in the absence of CO.

6.2. Experimental Setup

A general description of the SFG experimental setup has been given in chapter 3. In this experiment a different optical parametric system than described in chapter 3 was used, but the setup and function was similar. The fundamental from the Nd:YAG laser pumped a home built OPG/OPA system generating a tunable IR source in the 2-8 μm range. For 2-4 μm two $LiNbO_3$ crystals were used in an OPG/OPA stage, while in the 5 to 8 μm range the OPG/OPA stage consisted of two BBO crystals followed by a $AgGaS_2$ in a difference mixing stage. The second harmonic output (532nm) was used as the fixed visible laser beam in the SFG experiment. For SFG measurement, the green and the infrared beams were all p-polarized and their pulse energies at the surface were 250μJ for the green, 100μJ for the 2-4μm range and 80μJ for the 5-8 μm range. Their incident angles on the sample were 55º and 60°, respectively. Two energy meters were used to monitor the intensity of the infrared beams for normalization purposes.

An ultrahigh vacuum- high pressure (UHV-HP) system with a base pressure less than 3 x 10^{-10} Torr was used for sample preparation, which allowed for cleaning and characterization of the Pt(111) crystal in UHV and later transfering it under UHV conditions to the high pressure reaction cell for the SFG measurements. The Pt(111) crystal was cleaned by 12 minutes cycles of Ar^+ sputtering at 3x10^{-5} Torr Ar pressure followed by heating to 1133K in 5x10^{-7} Torr of O_2 for 2 minutes and annealing in

vacuum for an additional two minutes. CO (>99%, Scott Specialty Gases) was purified through a liquid nitrogen cold trap before used and ethylene purchased from Matheson was used directly without further purification. After the last cycle of cleaning and annealing, the Pt(111) crystal was first exposed to saturation coverage of CO or ethylene depending on the experimental requirements. The sample was then transferred to the high-pressure reaction cell where the SFG spectra were collected at room temperature for the coadsorption studies. During ethylene hydrogenation reaction, both SFG spectra and gas phase composition (using gas chromatography) were monitored at the same time. To obtain proper resonance peak position, the sum frequency signal I_{SFG} was fitted into Eq. 6.1 described in chapter 2.

$$I(\omega_{sum}) \propto \left| \chi_{NR} + \sum_q \frac{A_q e^{i\theta_q}}{\omega_{IR} - \omega_q + i\Gamma_q} \right|^2 \qquad (6.1)$$

6.3. Results

CO/ethylene coadsorption study

It is known that the vibrational frequency of CO adsorbed on the transition metal surface can be used to reveal information about CO adsorption site and CO bond strength. [15-20] To investigate the influence of coadsorbed ethylene to the CO bonding, the Pt(111) surface was first pretreated with 10L (10^{-6} Torr s) of ethylene at 330K. Under such condition, the Pt(111) surface was covered with a saturated monolayer of ethylidyne molecules (θ = 0.25ML). Figure 6.1-2 shows the surface vibrational spectra taken from

the ethylidyne pretreated surface at various CO pressures. When the ethylidyne pretreated surface was exposed to 10^{-7} Torr of CO, a resonance feature around 2020 cm^{-1} with a very broad linewidth was observed (figure 6.1). This peak was about 75 cm^{-1} red-shifted from the infrared absorption frequency of the a-top CO on clean Pt(111) surfaces. The vibrational signature of ethylidyne can be seen by the resonance feature around 2880 cm^{-1} (figure 6.2), which can be assigned to the symmetric CH_3 stretching mode of the ethylidyne molecules. This resonance feature was similar to those observed for pure ethylidyne adsorbed on Pt(111) surface. The CO vibrational peak grew as the CO pressure increased and it became sharper and shifted toward higher frequency. At the same time, the symmetric CH_3 stretching intensity decreased. In the high CO pressure region (>1 Torr), no clear resonance peak could be identified. However, some resonant features in the CH stretching region recovered after evacuating the high-pressure CO from the reaction cell.

The disappearance of CH stretching peak might indicate that high pressure CO displace the ethylidyne molecules from the Pt(111) surface. To determine the composition of the surface species, TPD spectra were taken at various CO dosages on the ethylidyne pretreated Pt(111) surface as shown in figure. 6.3. In the presence of CO, ethylidyne TPD spectrum showed a hydrogen desorption peak (mass 2) around 530K slightly higher than previous observations for the ethylidyne dehydrogenation temperature at around 500K. [14,21,22] A shoulder around 480K was observed when ethylidyne molecules coadsorbed with CO. At this temperature desorption peak mass 28 and 27 were also observed. In the presence of high pressure CO (>1 Torr), the major hydrogen desorption peak was shifted to 550K and its integrated intensity decreased

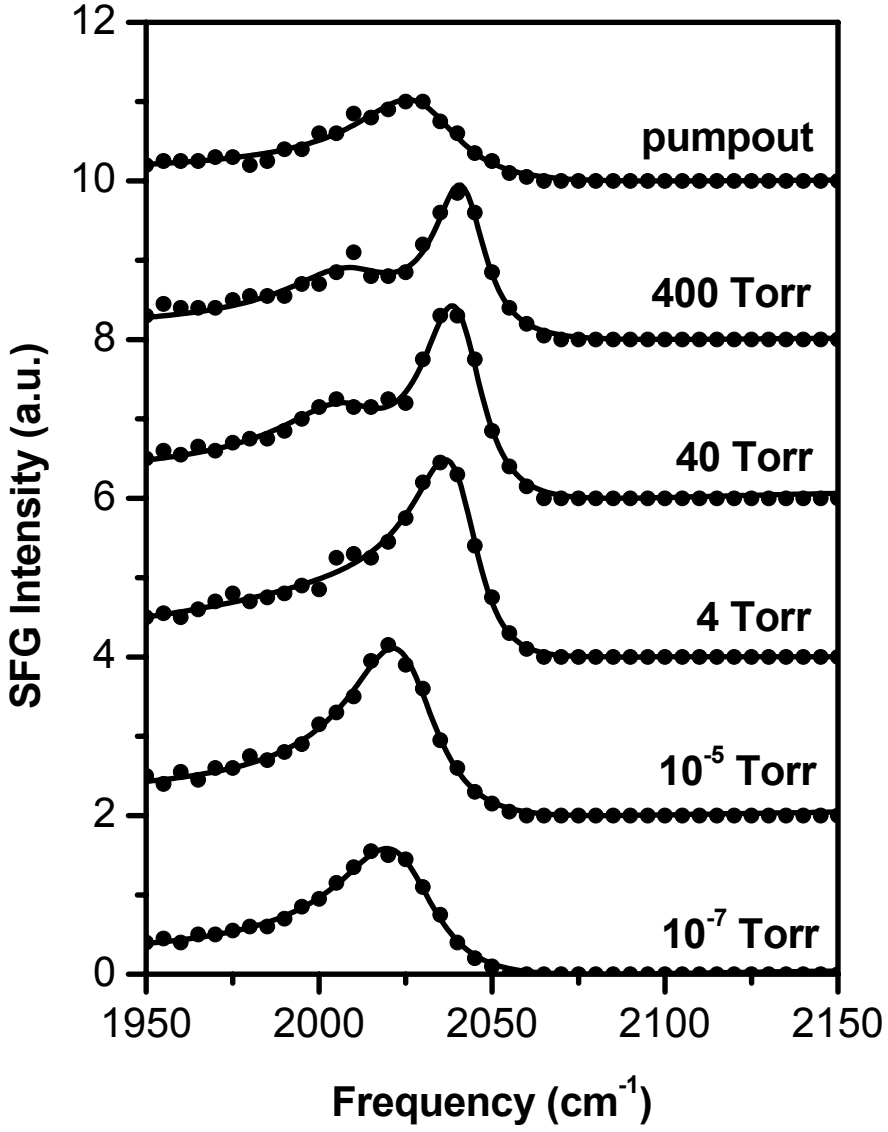

Figure 6.1. SFG spectra, in the CO region, of Pt(111) surface pretreated with 10 L ethylene at 330K at various CO pressures. Circles are experimental data and solid lines are fitted curves using Eq 6.1.

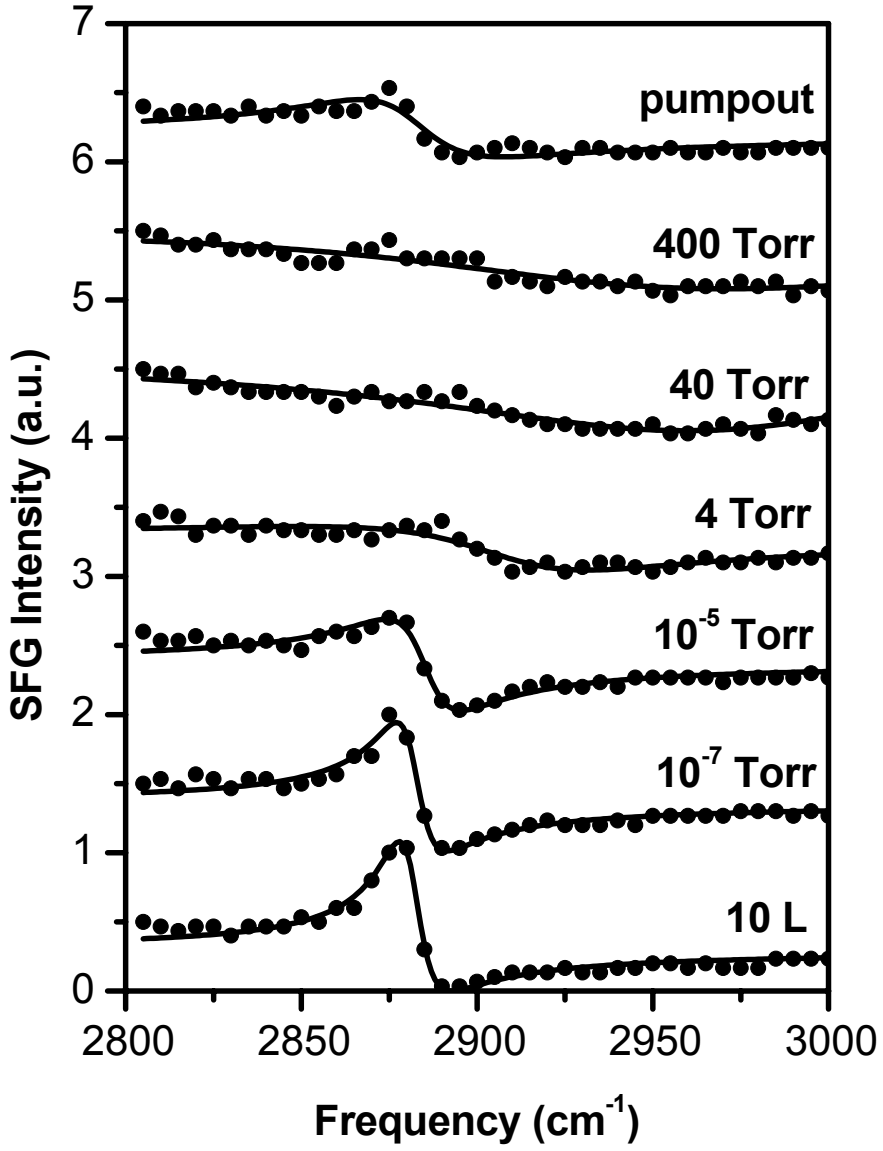

Figure 6.2. SFG spectra, in the CH region, of Pt(111) surface pretreated with 10 L ethylene at 330K at various CO pressures. Circles are experimental data and solid lines are fitted curves using Eq 6.1.

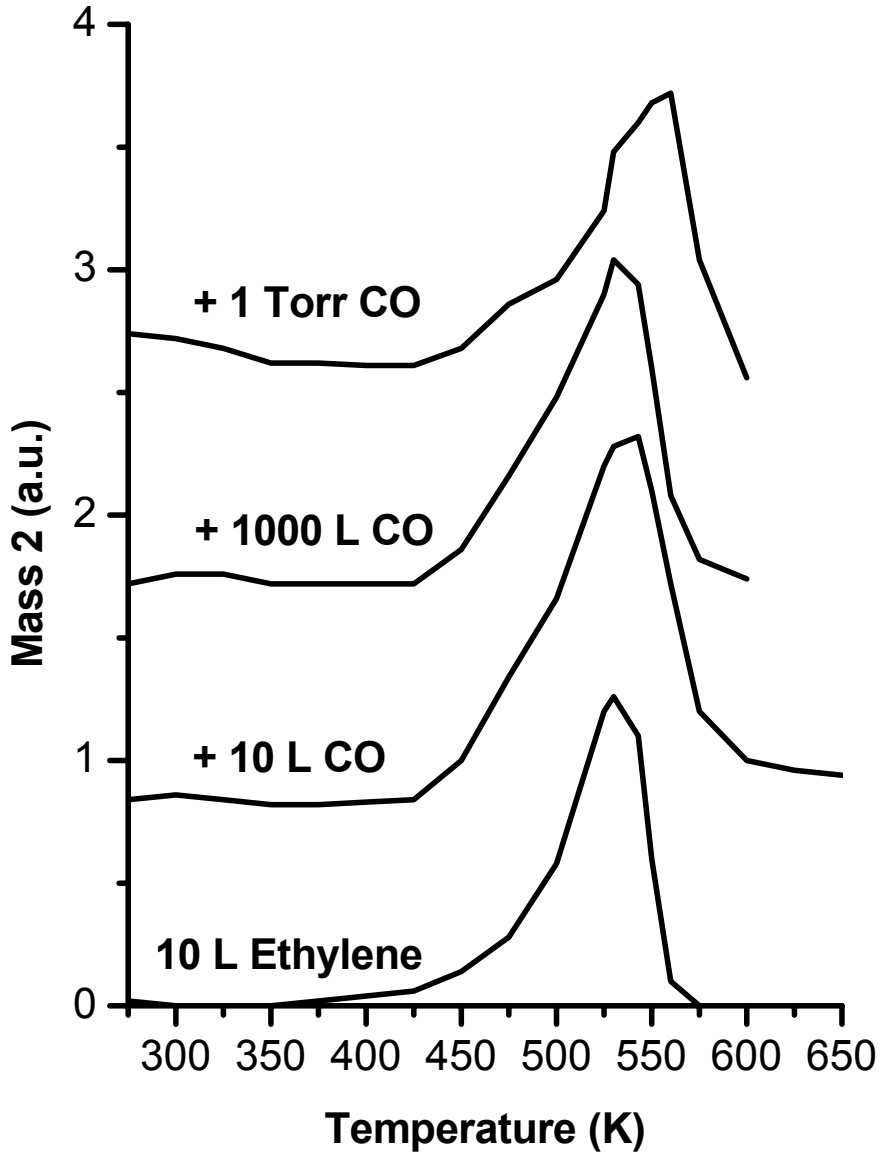

Figure 6.3. TPD (mass 2) spectra from the ethylene pretreated Pt(111) at different CO dosages.

about 25% indicating high pressure CO only displace some of the ethylidyne molecules on the surface.

To complete the coadsorption study, the coadsorption effect in the presence of high pressure ethylene have also been studied. In this experiment, the Pt(111) surface was first pretreated with 5L CO at 300K forming a saturation layer of CO on the surface (θ = 0.5) and then ethylene was slowly introduced to the high pressure cell. At 10^{-7} Torr of ethylene, a CO resonance peak around 2095 cm^{-1} was observed as shown in figure 6.4. As the ethylene pressure increased, the a-top CO peak position red-shifted to 2080 cm^{-1} while the peak intensity remained roughly the same. In the CH stretching region (figure 6.5), only a very weak peak around 2880 cm^{-1} with a shoulder around 2920 cm^{-1} was observed at all time. No spectral evolution was observed, which suggest that ethylene molecule cannot absorb on the Pt(111) surface when the surface is covered with a monolayer of CO.

CO poisoning of the ethylene hydrogenation catalytic reaction on the Pt(111) surface

To understand how CO molecules poison the ethylene hydrogenation reaction, the Pt(111) surface was pretreated with 10^{-7}, 10^{-5}, 0.1, and 3 Torr of CO. Then 10 Torr of ethylene and 100 Torr of hydrogen and 650 Torr of argon were added to the high pressure reaction cell. At low CO dosage, the ethylene hydrogenation rate increased slightly compared to those observed in the absence of CO. At high pressure CO (>0.1 Torr), no ethane product was observed at room temperature. The poisoning effect can be clearly seen from figure 6.6 where the ethylene hydrogenation reaction was terminated by

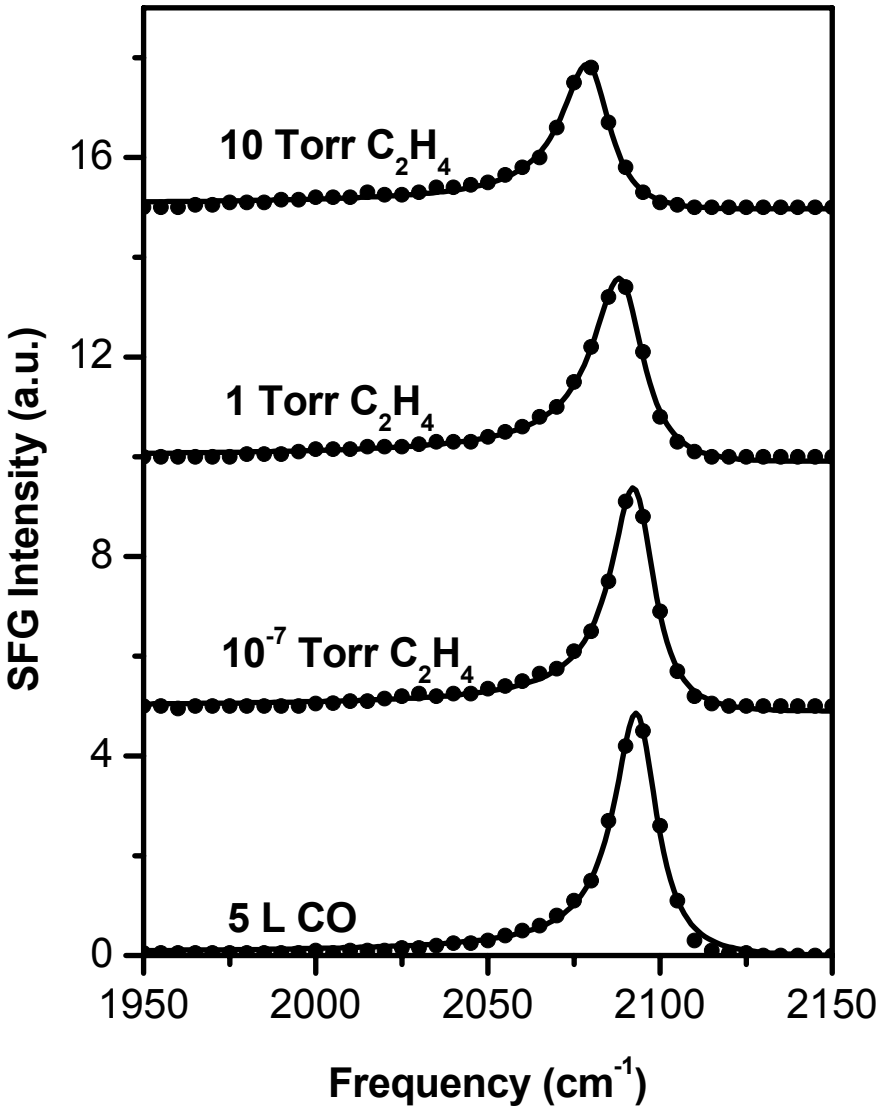

Figure 6.4. SFG spectra of the Pt(111) surface pretreated with 5 L CO at 300K in the CO stretching region at various ethylene pressures. Circles are experimental data and solid lines are fitted curves using Eq 6.1.

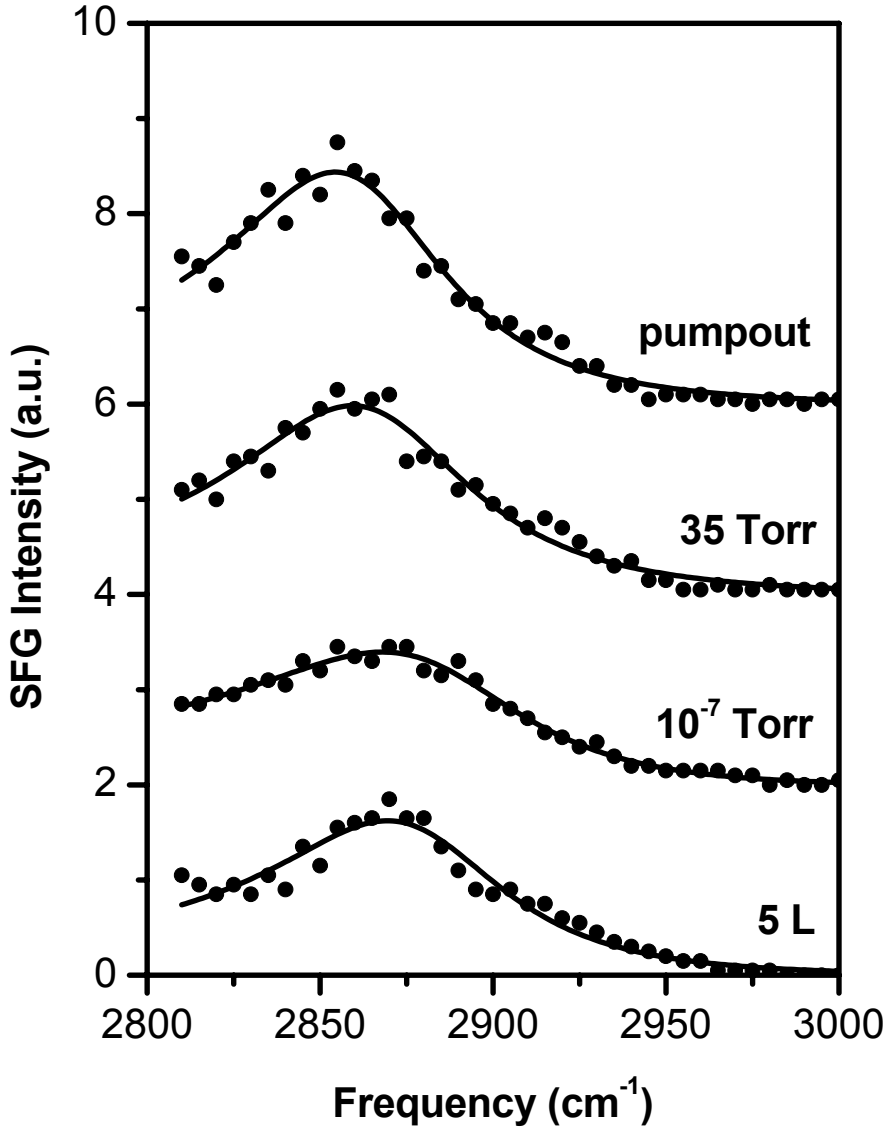

Figure 6.5. SFG spectra of the Pt(111) surface pretreated with 5 L CO at 300K in the CH stretching region at 5L, 10^{-7} Torr, 35 Torr of ethylene and after evacuating gas phase ethylene (pressure $>10^{-8}$ Torr). Circles are experimental data and solid lines are fitted curves using Eq 6.1.

Figure 6.6. The conversion efficiency of ethylene hydrogenation reaction, 10 Torr

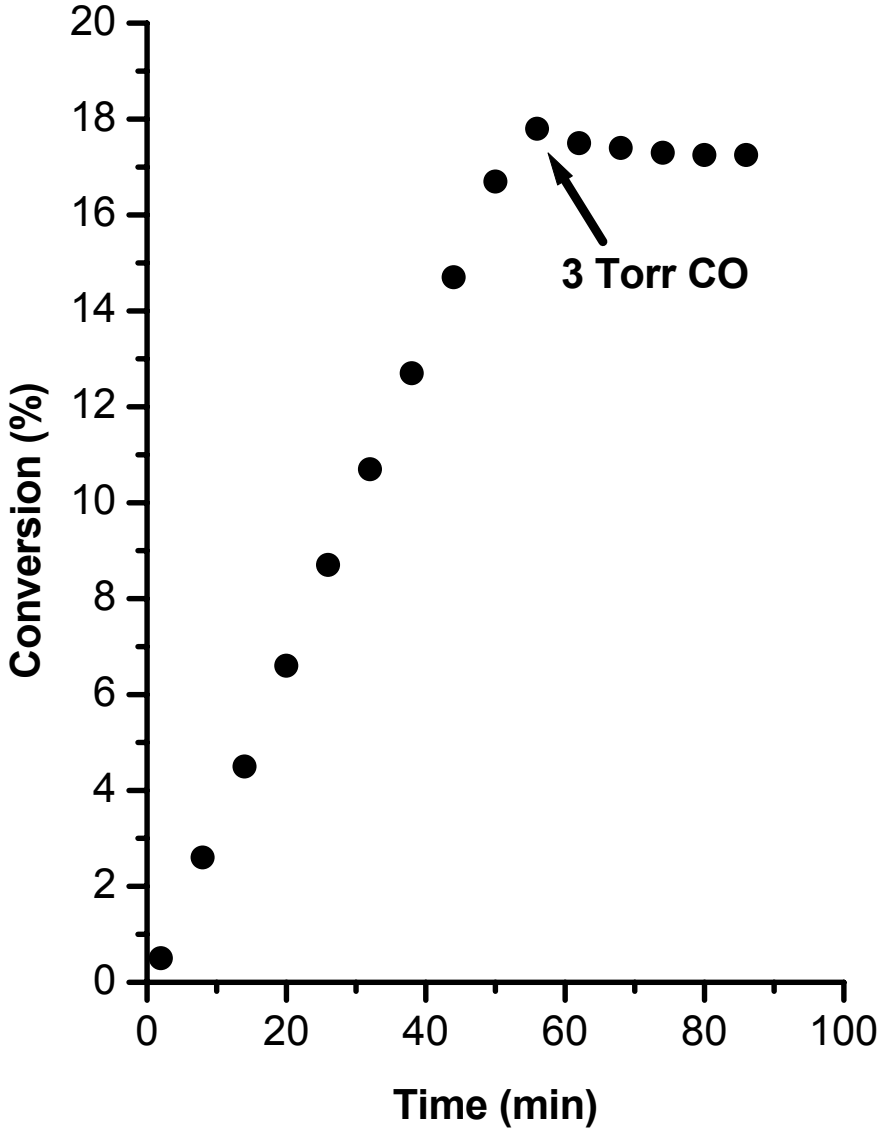

ethylene, 100 Torr hydrogen and 650 Torr argon. No further ethane production upon the introduction of 3 Torr CO.

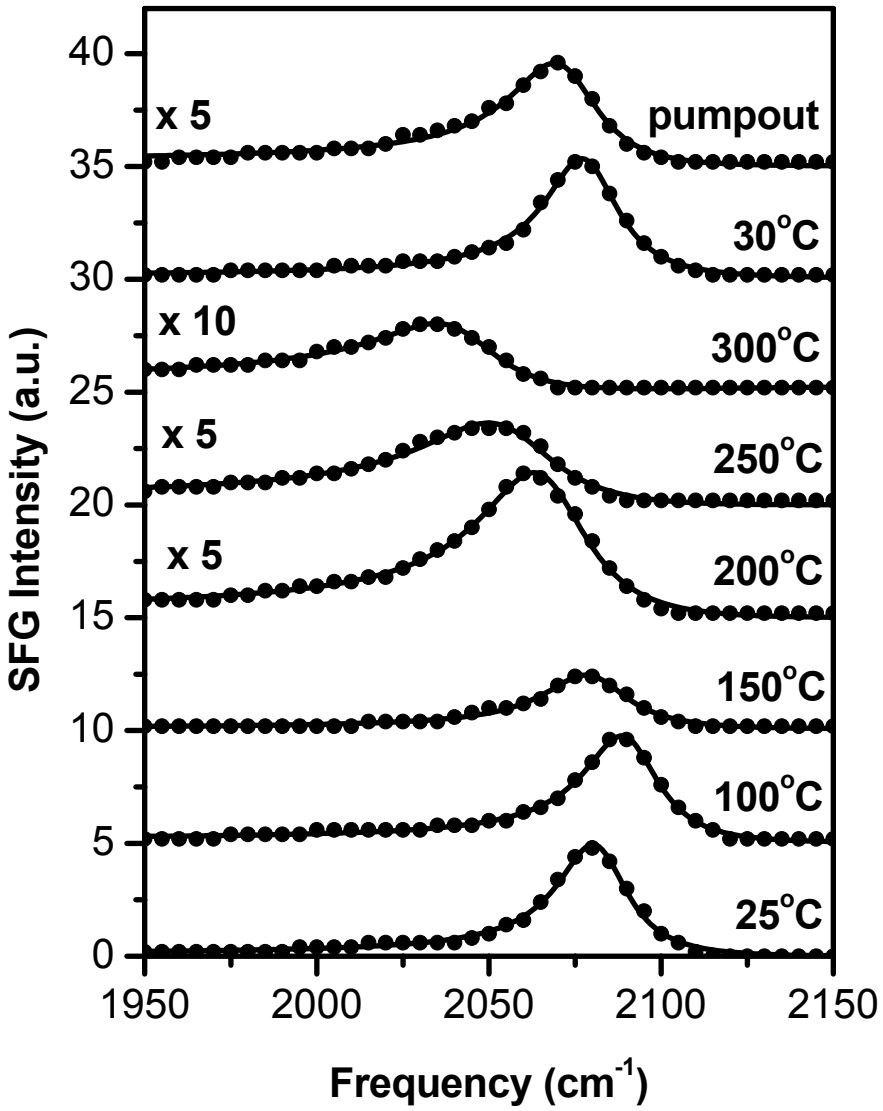

Figure 6.7. SFG spectra of the Pt(111) surface during the ethylene hydrogenation reaction in the presence of 3 Torr of CO at various temperatures. Shown here is only the CO stretching region. Gas phase composition is 3 Torr of CO, 10 Torr of ethylene, 100 Torr of hydrogen and 650 Torr of argon.

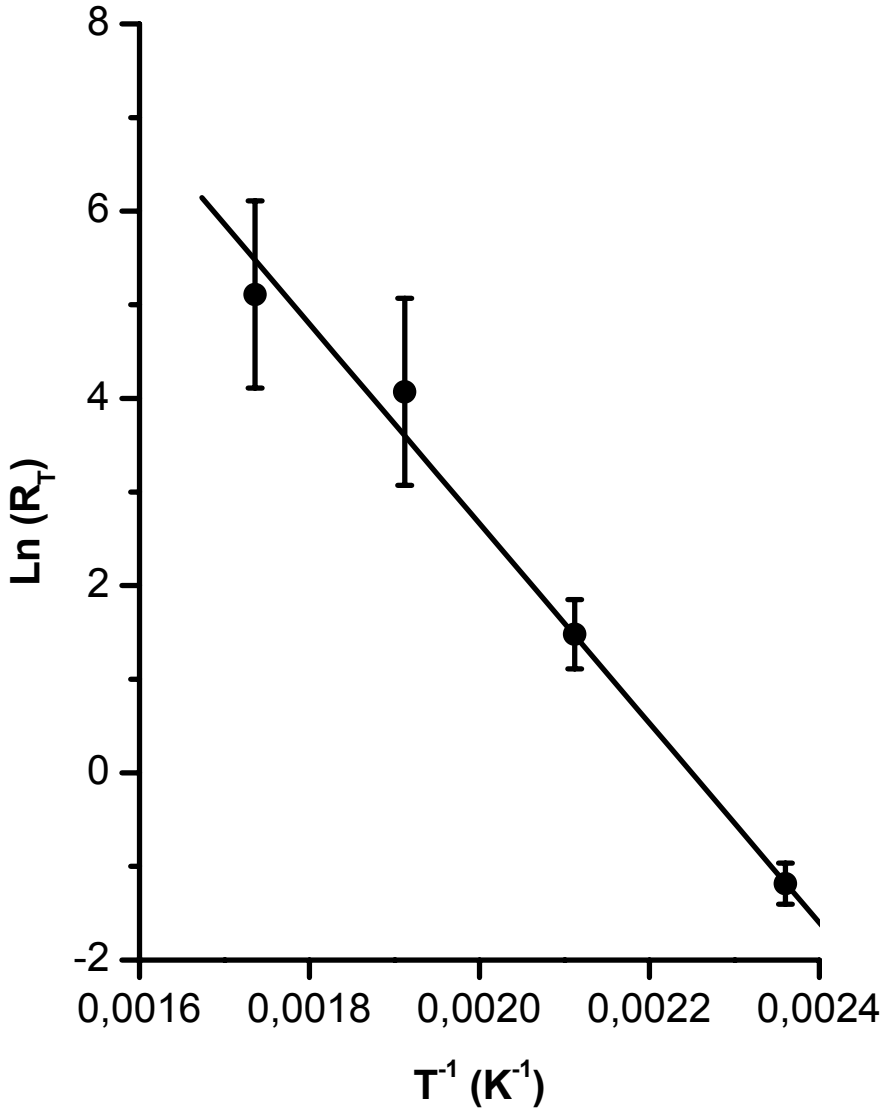

Figure 6.8. Activation energy of the CO poisoned ethylene hydrogenation reaction was calculated to be 20.5 ± 2 kcal/mole using reaction turn over rate at temperatures higher than 400K.

introduction of 3 Torr of CO. The reaction product, ethane, was only detected at higher temperatures (T>400K). Figure 6.7 shows the surface vibrational spectrum in the CO stretching region under reaction conditions in the presence of 3 Torr of CO at various temperatures. No change in CO peak intensity was observed at low temperature. At higher temperature, the CO peak red-shifted and decreased in intensity. Similar behavior was observed for pure CO adsorbed on the Pt(111) surface. [23] The reaction turnover rates above 423K were used to determine the activation energy for the CO poisoned ethylene hydrogenation reaction (figure 6.8). The activation energy was calculated to be 20.5 ±2 kcal/mol, which was much higher than the 10.8 kcal/mol activation energy needed for the ethylene hydrogenation on the Pt(111) in the absence of any CO. [24]

6.4. Discussion

CO is known to adsorb intact on the Pt(111) surface under UHV conditions forming a c(4x2) structure at saturation coverage (θ = 0.5) at room temperature. [15,16,18,19] Both a-top and bridge CO molecules coexist in this configuration, which exhibits two distinct IR absorption peaks around 2095 and 1850 cm^{-1}. At high CO pressure, only the a-top CO peak was observed at 2095 cm^{-1} by the SFG technique. The disappearance of the bridge bonded CO peak was attributed to the strong temperature dependence of its linewidth, which reduced the SFG signal by one order of magnitude when temperature was increased from 150K to 300K. [25] When ethylidyne pretreated Pt(111) crystal was exposed to 10^{-7} Torr of CO at 300K, a broadened CO resonance was observed around 2020 cm^{-1} which showed a red-shift of 75 cm^{-1} compared to the a-top

CO peak at 2095 cm^{-1} on the clean Pt(111) surface. A CO stretching frequency in the 2000 cm^{-1} region can be assigned to the CO adsorbed on the a-top site indicating the presence of ethylidyne molecules CO still occupies the a-top position. This observation is different from those observed for Pd catalysts supported on the silica in which ethylidyne blocked the CO adsorption on the Pt(111) sites in Pd/SiO2 catalysts. [26]

There are three distinct effects [27] that can lead to the reduction in the CO in the stretching frequency for adsorbed CO in the presence of the ethylidyne: (1) reduction in dipole-dipole interaction; (2) vibrational Stark effect where the frequency shift in proportional to the electric field exerted on the CO by coadsorbed species; (3) charge back donation from the metal surface to the $2\pi^*$ orbital of adsorbed CO. Using isotopic dilution, it was found that the dipole-dipole coupling effect accounted for 15 cm^{-1} out of the observed 25 cm^{-1} shift in the ethylene pretreated Pt/SiO2 catalysts. [28] The Stark effect is important when CO is coadsorbed with a species that has a very large surface dipole moment. However, the surface dipole moment for ethylidyne molecules is relatively small (0.9 D on the Rh(111) surface). It was estimated that this surface dipole moment could generate a 30 cm^{-1} frequency shift. [27] Therefore, the rest of the frequency shift could be attributed to the surface charge transfer. Ethylidyne is known to be an electron donor. When ethylidyne coadsorbed with CO, the excess electron charge on the surface will weaken the CO bond through d-π back donating mechanism. [28] As a result, the vibrational frequency of the a-top CO coadsorbed with ethylidyne could show a large red-shift. This result indicates that CO adsorption on the hydrocarbon surface could lead to the weakening of CO bond, which is a prerequisite of catalytic CO hydrogenation. In fact, in one of our previous measurements, we have observed CO

dissociation on the Pt(111) at the high CO pressure and high temperature. The observed CO peak frequency also showed a large red-shift, which was the result of the coadsorption of CO with surface carbon.

As the CO pressure increased, the CO peak intensity increased indicating increase in the surface CO concentration (figure 6.1), which also caused frequency shift towards higher frequency due to the increase of CO-CO lateral interaction on the Pt(111) surface. In the same time, the CH_3 stretching intensity of ethylidyne decreased with increasing CO pressure. [30] The a-top CO peak intensity increases at the expense of the ethylidyne peak indicating that CO may displace ethylidyne molecules on the surface. At high CO pressure, no dominant resonance feature in the CH stretching region can be seen. One may conclude that CO molecules completely displace ethylidyne on the platinum surface. However, TPD spectra showed that after exposure to 1 Torr of CO, only 25% of ethylidyne molecules were displaced, the majority still stayed on the platinum surface. One possible explanation for the disappearance of the CH resonance feature at high CO pressure is that high pressure CO may induce disordering for ethylidyne molecules. Since the SFG technique is very sensitive to polar ordering, orientation disorder can cause SFG intensity to drop significantly. An alternative explanation for the disappearance of the CH resonance feature could be attributed to the modification of optical response in the presence of strong vibrational dipole moment pf the coadsorbed CO. [31,32]

When the Pt(111) surface was pretreated with CO, no noticeable change of vibrational spectra were observed as the pressure of ethylene was increased up to 35 Torr. This result indicates that in the presence of a monolayer of CO (θ = 0.5) at room temperature, ethylene cannot adsorb on the surface. The adsorption of ethylene requires

two platinum sites, which are blocked by the adsorbed CO. This site blocking effect may lead to the poisoning of the catalytic reaction that requires ethylene adsorption. In fact, no reactivity was found for the ethylene hydrogenation reaction at room temperature in the presence of 3 Torr of CO. The reaction product ethane was only observed at temperatures that were higher than the CO desorption temperature. This clearly indicates that CO is blocking the sites needed for the ethylene hydrogenation reaction to occur. At higher temperature, ethane was detected, however, the reaction rate was three orders of magnitude lower than the same reaction in the absence of high pressure CO. The activation energy measured in this CO poisoned ethylene hydrogenation reaction was 20.5 kcal/mol which was much higher than 10 kcal/mol needed for ethylene hydrogenation on the clean Pt(111) surface. This result suggests that the activation energy for such reaction is the heat of desorption of CO, which is to remove CO from the surface to allow ethylene adsorption and then hydrogenation on the platinum surface. It should be mentioned that the reactivity of ethylene hydrogenation on the Pt(111) surface was poisoned only at high CO pressure (>0.1 Torr). At low CO pressure (10^{-7}, 10^{-5} Torr), the ethylene hydrogenation rate increased slightly. One possible explanation is that high pressure hydrogen (100Torr) may react with or displace CO, which is supported by the disappearance of CO resonance feature upon the introduction of high pressure hydrogen in this CO pressure region.

6.5. Conclusions

When CO adsorbed on the ethylidyne pretreated surface its vibrational spectra red- shifted about 75 cm^{-1}, which is mainly due to the weakening of CO bond through d-π back donation from coadsorbed ethylidyne molecules. In the CO pretreated Pt(111) surface, the presence of high pressure ethylene does not change the vibrational spectra in the CH stretching region indicating that ethylene cannot adsorb on the surface that is covered by a monolayer of CO.

During the studies of catalytic ethylene hydrogenation in the presence of CO, it was found that CO poisons the catalytic reaction by site blocking effect up to 400K where CO desorbs from the Pt(111) surface. The measured apparent activation energy was 20.5 kcal/mol instead of 10 kcal/mol.

References:

(1) Paal, Z.; Somorjai, G.A. Promotors and Poisons, in : Ertl,G.; Knozinger, H.; Weitkamp, J. (Eds), Handbook of Heterogeneous Catalysis, Weiley-VCH, Weinhein, **1997**, p. 1084.

(2) Oudar, J.; Modeling experiments of poisoning on metals, in: Oudar, J.; Wise, H. (Eds), Deactivation and Poisoning of Catalysts, **1985**, Dekker, New York, p. 51.

(3) Cremer, P.S.; Sue, X.C.; Shen, Y.R.; Somorjai, G.A. *J. Am. Chem. Soc*, **1996**, *118*, 2942.

(4) Sue, X.C.; Cremer, P.S.; Shen, Y.R.; Somorjai, G.A. *Phys. Rev. Lett.* **1996**, *77*, 3858.

(5) Härle, H.; Lehnert, A.; Metka, U.; Volpp, H.R.; Willms, L.; Wolfrum, J.; *Appl. Phys. B* **1999**, *68*, 567.

(6) Katano, S.; Bandara, A.; Kubota, J.; Onda, K.; Wada, K.; Domen, K.; Hirose, C. *Surf. Sci.* **1999**, *428*, 337.

(7) Tadjeddine, A.; Peremans, A. *Surf. Sci.* **1996**, *368*, 377.

(8) Baldelli, S.; Mailhot, G.; Ross, p.; Shen, Y.R.; Somorjai, G.A. *J. Phys. Chem. B* **2001**, *105*, 654.

(9) Gragson, D.E.; McCarty, B.M.; Richmond, G.L. *J. Phys. Chem.* **1996**, *100*, 14272.

(10) Baldelli, S.; Schnitzer, C.; Shultz, M.J.; Cambell, D.J. *J. Phys. Chem. B* **1997**, *101*, 10435.

(11) Miranda, P.B.; Shen, Y.R. *J. Phys. Chem. B* **1999**, 103, 3292.

(12) Walker, R.A.; Gruetzmacher, J.A.; Richmond, G.L. *J. Am. Chem. Soc.* **1998**, *120*, 6991.

(13) Cremer, P.; Stanners, C.; Nietmansverdriet, J.W.; Shen, Y.R.; Somorjai, G.A. *Surf. Sci.* **1995**, *328*, 111.

(14) Zaera, F. *Langmuir* **1996**, *12*, 88.

(15) Hayden, B.E.; Bradshaw, A.M. *Surf. Sci.* **1983**, *125*, 787.

(16) Trenary, M.; Uram, K,J; Yates, J.T.; *Surf. Sci.* **1985**, 157, 512.

(17) Kuhn, W.K.; Szanyi, J.; Goodman, D.W.; *Surf. Sci.* **1992**, *274*, L611.

(18) Hollins, P.; Pritchard, J. *Prog. Surf. Sci.* **1985**, *19*, 275.

(19) Tushaus, M.; Schweizer, E.; Hollins, P.; Bradshaw, A.M. *J. Electron Spectrosc. Related Phenomena* **1987**, *44*, 305.

(20) Crossley, A.; King, D.A. *Surf. Sci.* **1977**, *68*, 528.

(21) Salmeron, M.; Somorjai, G.A. *J. Phys. Chem.***1982**, *86*, 341.

(22) Creighton, J.R.; White, J.M. *Surf. Sci.* **1983**, *129*, 327.

(23) Kung, K.Y.; Chen, P.; Wei, F.; Shen, Y.R.; Somorjai, G.A. *Surf. Sci.* **2000**, *463*. L627.

(24) Zaera, F.; Somorjai, G.A. *J. Am. Chem. Soc.* **1984**, *106*, 2288.

(25) Klunker, C.; Balden, M.; Lehwald, S.; Daum, W. *Surf. Sci.* **1996,** *360*, 104.

(26) Beebe, T.P.; Yates, J.T. *Surf. Sci.* **1986**, *173*, L606.

(27) Mate, C.M.; Kao, C.T.; Somorjai, G.A. *Surf. Sci.* **1988**, *206*, 145.

(28) Stoop, F.; Toolenaar, F.J.C.M.; Ponec, V. *J. Catal.* **1982**, *73*, 50.

(29) Blyholder, G. *J. Phys. Chem.* **1964**, *68,* 2772.

(30) Chen, P.; Kung, K.Y.; Shen, Y.R.; Somorjai, G.A. *Surf. Sci.* **2001**, *494*, 289.

(31) Ainsworth, M.K.; McCoustra, M.R.S.; Chesters, M.A.; Sheppard, N.; de la Cruz, C. *Surf. Sci.* **1997**, *437*, 9.

(32) Blackman, G.S.; Kao, C.T.; Bent, B.E.; Mate, C.M.; van Hove, M.A.; Somorjai, G.A. *Surf. Sci.* **1988**, *207*, 66.

Chapter 7. Heat of adsorption of CO on Pt(111)

7.1. Introduction

The adsorption of CO on Pt(111) has been subjected to a number of studies using various techniques, such as calorimetry, TPD, LEED, infrared adsorption spectroscopy (IRAS), etc. [1-6], and more recently SFG. [7-11] The knowledge of adsorption behavior is essential to gain an understanding on the heat of adsorption and adsorption geometry, which are key elements of surface chemistry. [12] SFG offers a unique venue to study molecular adsorption on surfaces, in particular the molecular layer directly adsorbed on the surface. [13-15] The SFG results could be employed to perform *in situ* study of the adsorbed species.

By correlating the integrated TPD signal and SFG intensity of CO coverage on Pt, [8] Härle et al. obtained a linear relationship of CO coverage on a Pt foil versus SFG intensity. A different correlation was observed for CO adsorption on Ni(111) by Bandara et al. [16] In the latter case, a non-linear relationship between SFG intensity from a-top (or bridge site) CO and overall coverage was obtained. Such variation is indicative of the complexity of adsorption behavior of CO molecules on metal surfaces. However, the above results could serve to establish the relationship between actual surface coverage (up to 1 monolayer) It should be noted that the SFG intensity depends on several parameters, such as coverage, orientation, cross-section for the SFG process, etc, and that the relationship between the intensity and coverage needs to be confirmed experimentally with a supplementing technique, such as temperature programmed desorption. In the case

of CO on platinum the SFG intensity of the a-top CO was found to depend linearly in the coverage as shown by Härle. [10] Provided that a relationship can be determined, it enables studies on general properties of adsorption, namely the isotherm behavior and subsequently heat of adsorption.

In this work, we obtained the adsorption isotherm of CO on Pt(111) surface in the temperature range of 373K to 463K using SFG. Using a Langmuir expression, suitable for monolayer adsorption, heat of adsorption was extracted from the isotherms. The heat of adsorption close to saturation was determined to 98kJ/mol, which is in close agreement with values obtained by calorimetry, LEED and TPD. [17,18]

7.2. Experimental Setup

The experiments were carried out in a UHV chamber, which allowed surface studies over a pressure range from 10^{-10} Torr (base pressure) to 10^{-4} Torr. The system was equipped with a retarding field analyzer (RFA), for Auger electron spectroscopy (AES) and low-energy electron diffraction (LEED) analysis. The chamber was further equipped with an ion bombardment gun for cleaning purposes and a mass spectrometer for gas analysis. The sample was mounted on the sample holder where it could be resistively heated to 1400K or cooled by a flow of liquid nitrogen down to 170K.

The Pt(111) sample was cut, oriented and polished by normal procedures. The platinum was cleaned by several cycles of Ar ion bombardment followed by annealing in $5x10^{-7}$ Torr of oxygen at 1100K. The crystal cleanliness and structure was confirmed with AES and LEED. CO was introduced through a leak valve and SFG spectra were

recorded at different temperatures as a function of pressure. Between each data set the Pt crystal was annealed 2 minutes at 1100K with an oxygen pressure of $5x10^{-7}$ Torr followed by 2 minutes at 1100K in vacuum. This procedure ensured a clean and reproducible surface for CO adsorption.

The SFG setup was similar to the one described in chapter 3. Again both beams were p-polarized but in this case the incident angles were 50° and 60° for the visible and IR. The intensity of the input beams were well below intensities needed for photo-induced desorption of CO and no changes in the spectra could be seen as a function of time. The experimental data were fitted to Eq. 7.1, described in chapter 2, using a least squares method, to extract the values of parameters, such as peak position, peak width, amplitude, phase and non-resonant background.

$$I(\omega_{sum}) \propto \left| \chi_{NR} + \sum_q \frac{A_q e^{i\theta_q}}{\omega_{IR} - \omega_q + i\Gamma_q} \right|^2 \tag{7.1}$$

7.3. Results

SFG spectra of CO adsorbed on Pt(111) were recorded in the pressure range of $1x10^{-8}$ to $3x10^{-5}$ Torr by scanning the IR frequency between 2000 cm^{-1} and 2200 cm^{-1}. The temperature was 373K for the first set of pressures and it remained constant through the pressure range. After one complete measurement of SFG spectra versus pressure, the sample was cleaned by annealing in oxygen at 1100K. When the sample had cooled down, the surface cleanliness was checked by AES and CO was reintroduced. A new set of SFG spectra versus pressure were recorded at a higher temperature. Pressure

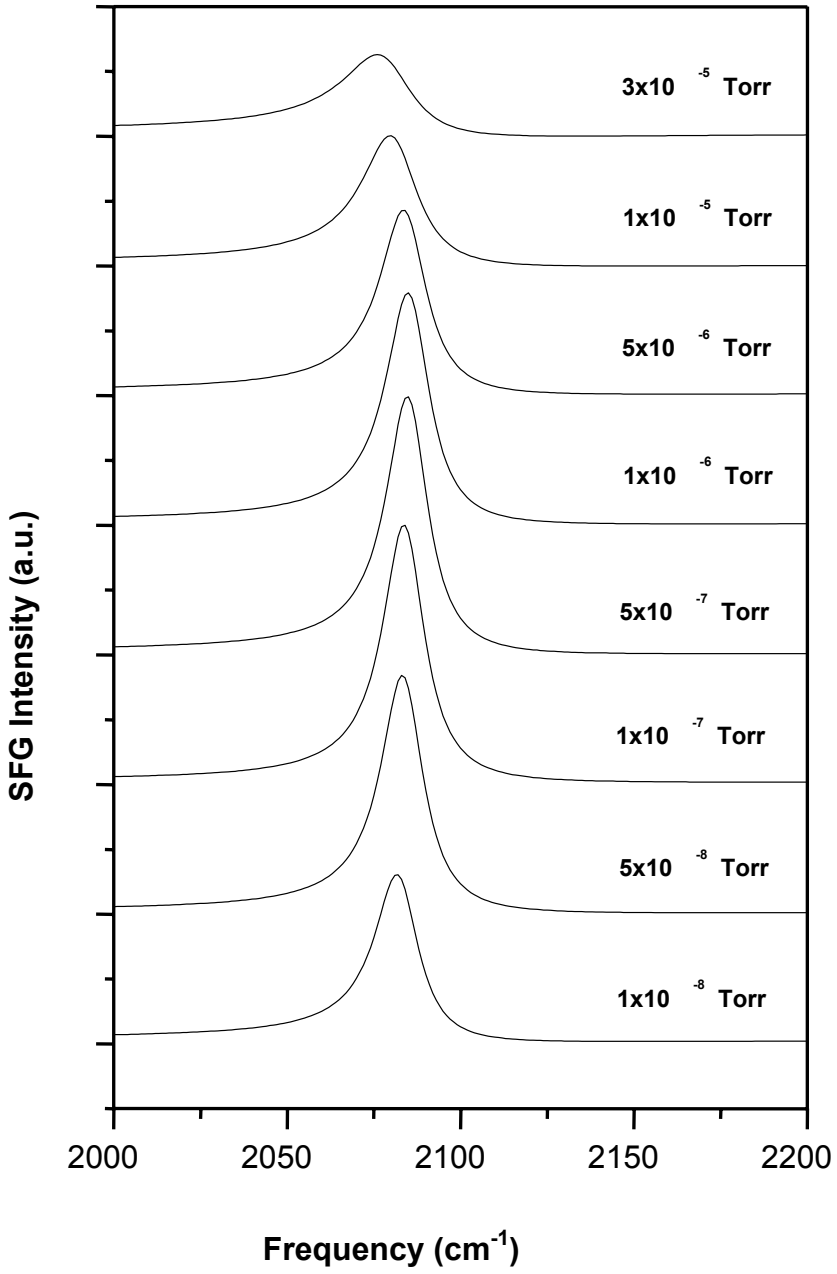

Figure 7.1. Fitted SFG spectra of CO adsorbed on Pt(111). The CO pressure was increased from $1x10^{-8}$ Torr to $3x10^{-5}$ Torr while holding the temperature constant at 403K.

dependent SFG spectra were recorded at 7 different temperatures between 373K and 463K. Shown in figure 7.1 is one set of SFG spectra, recorded at 403K, where the single peak corresponds to CO adsorbed on a-top sites on Pt(111). It can be seen from figure 7.1 that the SFG intensity increased as the pressure is increased from $1x10^{-8}$ Torr to $1x10^{-7}$ Torr. Going above $1x10^{-7}$ Torr in pressure, the SFG intensity decreased continuously up to $3x10^{-5}$ Torr, which is the highest pressure investigated in this study. By fitting the data to Eq. 7.1 amplitude and peak position were determined. The trend for the amplitude follows the trend in intensity, where the maximum amplitude was recorded at $1x10^{-7}$ Torr. The peak position for a-top CO is determined to 2083 cm^{-1} at $1x10^{-8}$ Torr. It shifted to 2086 cm^{-1} at $1x10^{-6}$ Torr where after it came down to 2079 cm^{-1} at $3x10^{-5}$ Torr.

SFG intensity and CO peak positions are both dependent on the surface coverage. In the pressure range studied in this experiment the surface reached saturation coverage, dictated by adsorption and desorption processes. At each pressure and temperature the adsorption and desorption will reach an equilibrium that will determine the surface coverage. Increased pressure favors higher surface coverage, while higher temperature increases desorption and thereby lower the surface coverage. Data from each temperature have been fitted to Eq. 7.1 and the result can be seen in figure 7.2 where intensity and peak positions are plotted against pressure.

At room temperature CO is shown to reach saturation coverage at 10 Langmuir with a total surface coverage of 0.5 ML in a c(4x2) structure. [18] Consistent with the previous studies at room temperature we observed a CO saturated surface when holding the sample at a constant pressure of $1x10^{-8}$ Torr. The SFG spectra of CO showed no changes in intensity as the temperature was increased to 373K. As the temperature

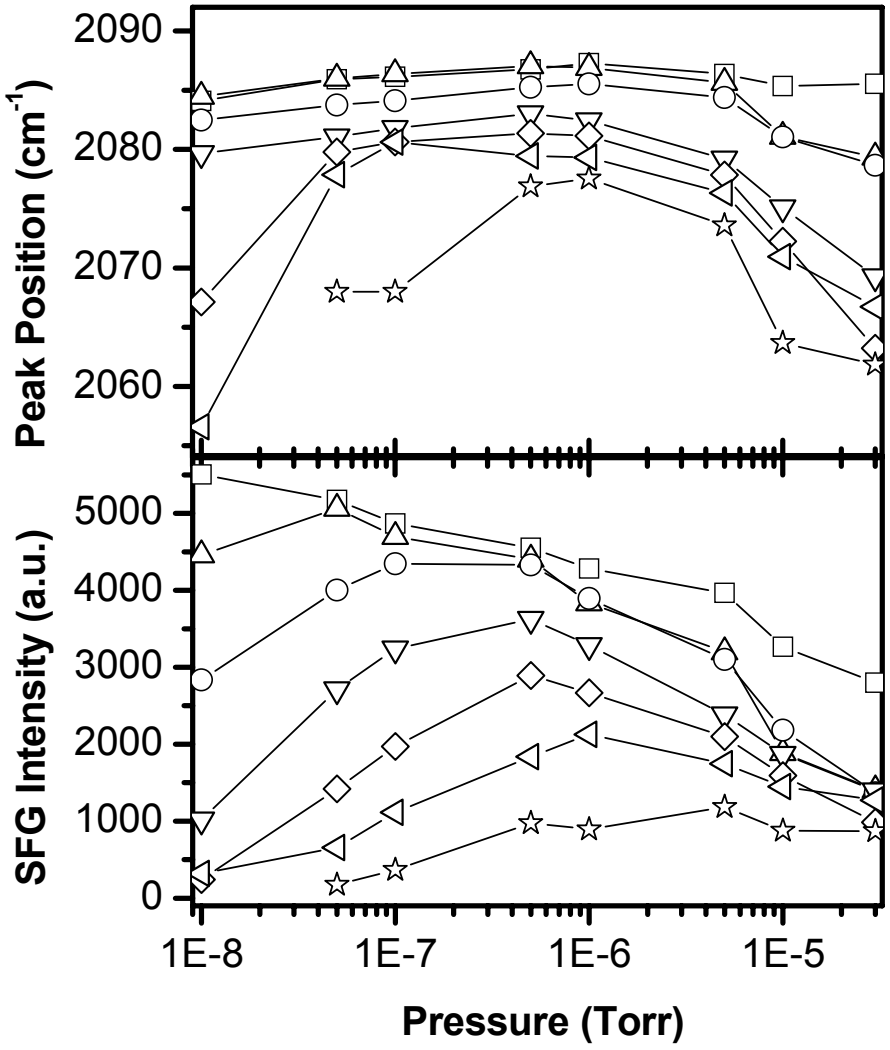

Figure 7.2. Peak position and SFG intensity for CO on Pt(111) are plotted against pressure. The measurements were repeated at 7 different temperatures with 15K increments between 373K and 463K, 〈 373K, ⎧ 388K, ⎪ 403K, ⎩ 418K, ⎨ 433K, ◁ 448K, ⎭ 463K. Solid lines are guides for the eye for each temperature.

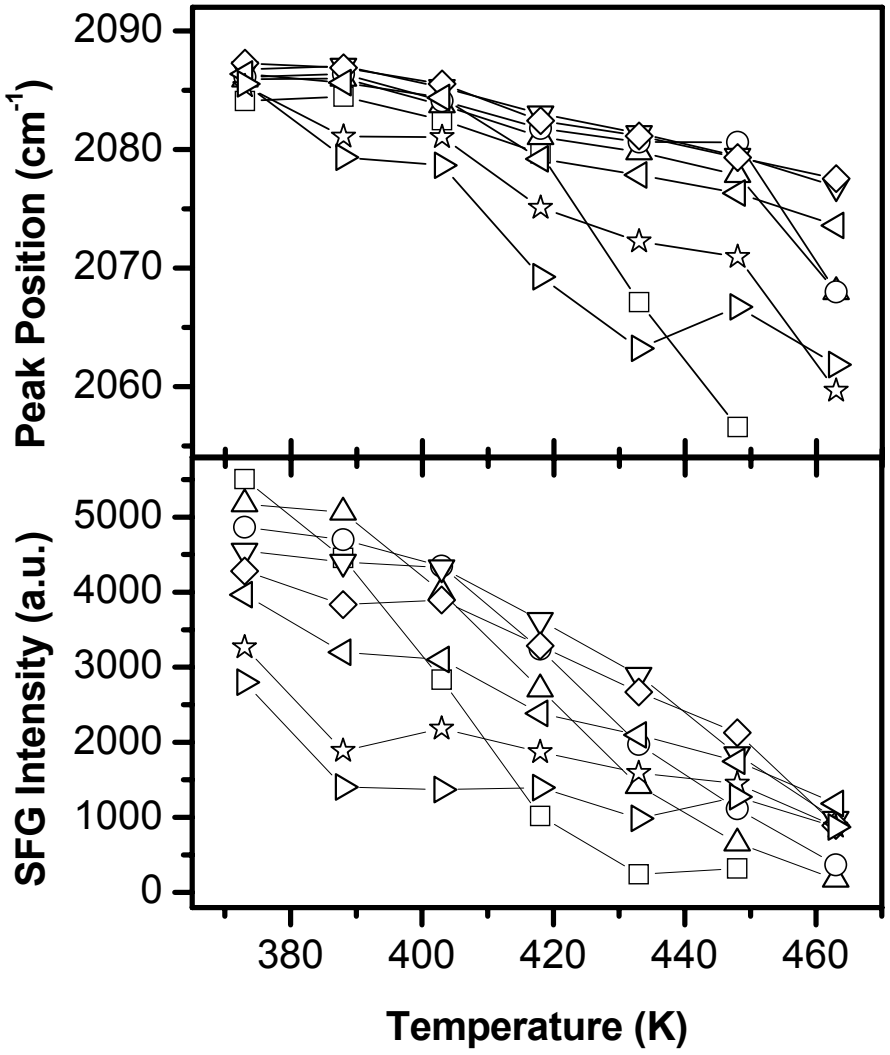

Figure 7.3. Peak position and SFG intensity for CO on Pt(111) are plotted against temperature. Data points were taken at 8 different pressures between $1x10^{-8}$ and $3x10^{-5}$ Torr, ⟨ $1x10^{-8}$ Torr, ⌠ $5x10^{-8}$ Torr, | $1x10^{-7}$ Torr, ⌡ $5x10^{-7}$ Torr, ⎨ $1x10^{-6}$ Torr, ◁ $5x10^{-6}$ Torr, ⎩ $1x10^{-5}$ Torr, ▷ $3x10^{-5}$ Torr. Solid lines are guides for the eye for each pressure.

increases, the desorption rate of CO increases. This results in a decrease of the surface coverage of CO characterized by a decrease in SFG signal intensity. This effect is illustrated in figure 3 where intensity and peak position (at constant pressure) are plotted for various temperatures.

7.4. Discussion

In this study we have used SFG to measure surface coverage of CO in Pt(111), which can be utilized to determine thermodynamic parameters, such as heat of adsorption. A linear relationship between SFG intensity of the a-top CO peak on Pt and the surface coverage has been proven by Härle at al. [8] This relationship can be used to determine surface coverage, in situ, under pressurized or flow systems. For CO on Pt(111), the heat of adsorption can be determined by looking at the increase in surface coverage from a corresponding increase in pressure at elevated temperatures. These data points are presented in figure 7.4. The maximum intensity of the a-top CO peak was normalized to 1 and it was assumed that, for each temperature, the maximum intensity corresponded to saturation coverage. A comparison could then be made between the relative changes in coverage at different temperatures and pressures. Surface coverage is close to saturation and Langmuir adsorption is assumed. The adsorption is described by Eq. 7.2, where σ is the surface coverage and b is a parameter that contains the flux of gases and the residence time further described by Eq. 7.3. P is the pressure and σ_0 is the surface coverage of a completely covered surface.

$$\frac{1}{\sigma} = \frac{1}{bP} + \frac{1}{\sigma_0} \tag{7.2}$$

$$b = \frac{N_A}{\sqrt{2\pi MRT}} \tau_0 \exp\left(\frac{\Delta H_{ads}}{RT}\right) \tag{7.3}$$

Figure 7.5 presents a linear Langmuir plot of σ^{-1} versus P^{-1}. The slope of the linear Langmuir plot is b^{-1}, which was obtained for various temperatures. By plotting ln(b) against T^{-1}, as illustrated in figure 7.6, the heat of adsorption, ΔH_{ads}, can be extracted from the slope of the linear fit, where the slope is $\Delta H_{ads}/R$. The value for the heat of adsorption close to saturation of CO on Pt(111) was determined to be 98kJ/mol, which is in accordance to values reported by King, (118kJ at 0.5ML, reduced down to 65kJ/mol at saturation) [17] and by Ertl (138kJ/mol at zero coverage and decreasing with coverage). [18] The close agreement validates the method of measuring heat of adsorption by SFG. In the case of CO on Pt(111) the relationship between SFG intensity and coverage has been proven to be linear. Other systems may have more complicated relationships. However, the use of SFG as a tool to measure thermodynamic parameters can be extended to those systems provided a specific relationship is established. The isotherm measurements by SFG could also be beneficial for studying more complex adsorption systems, such as co-adsorptions.

In figure 2 and figure 3 several trends in signal intensity and peak positions versus pressure or temperature are observed. At 10^{-8} Torr, saturation coverage is obtained at room temperature. The coverage has previously been determined to correspond to a 0.5 ML coverage in a c(4x2) structure on Pt(111). When increasing the temperature to 373K, while maintaining the pressure at 10^{-8} Torr, no changes in signal intensity were observed. The results imply that the surface remains at full coverage up to 373K. A further increase in temperature leads to a higher desorption rate, which affects the coverage. This is

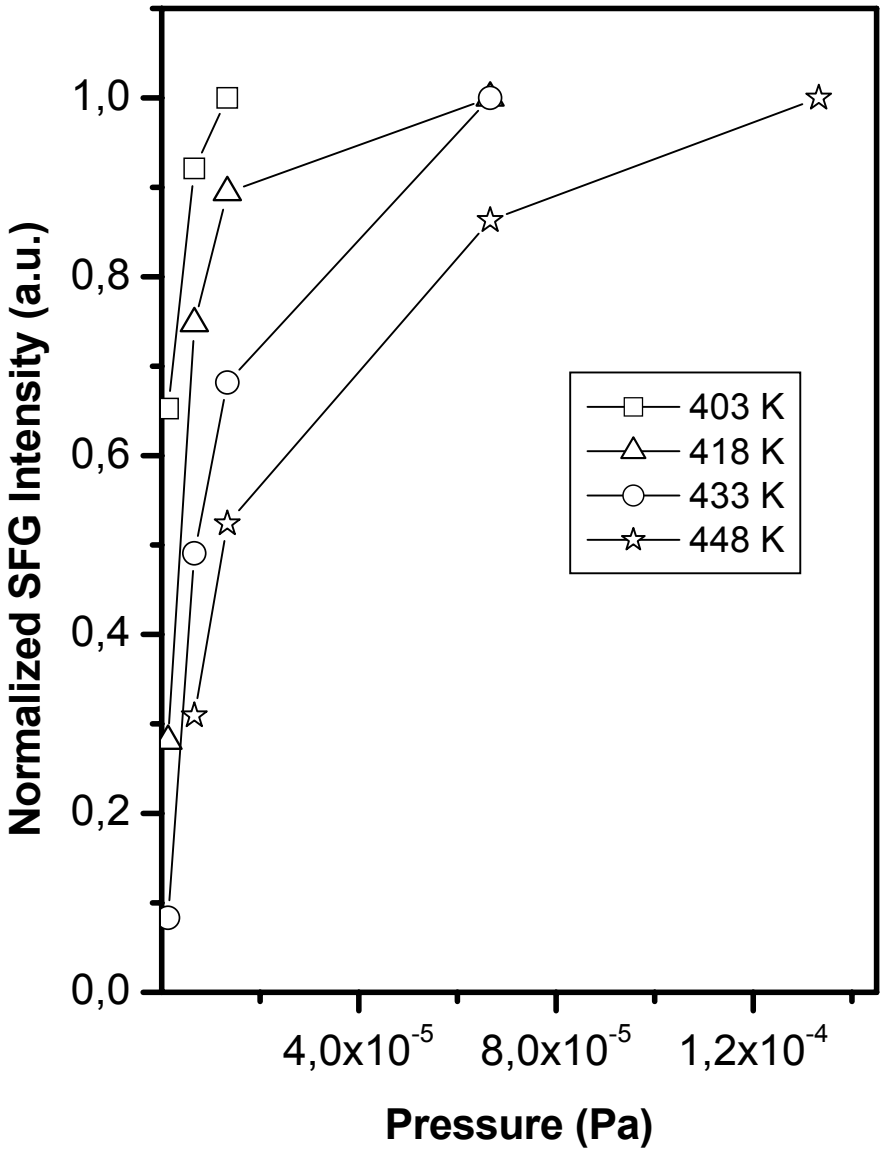

Figure 7.4. SFG intensity of CO on Pt(111) is plotted against pressure. The maximum intensity for each temperature has been normalized to 1. Solid lines are guides for the eye for each temperature.

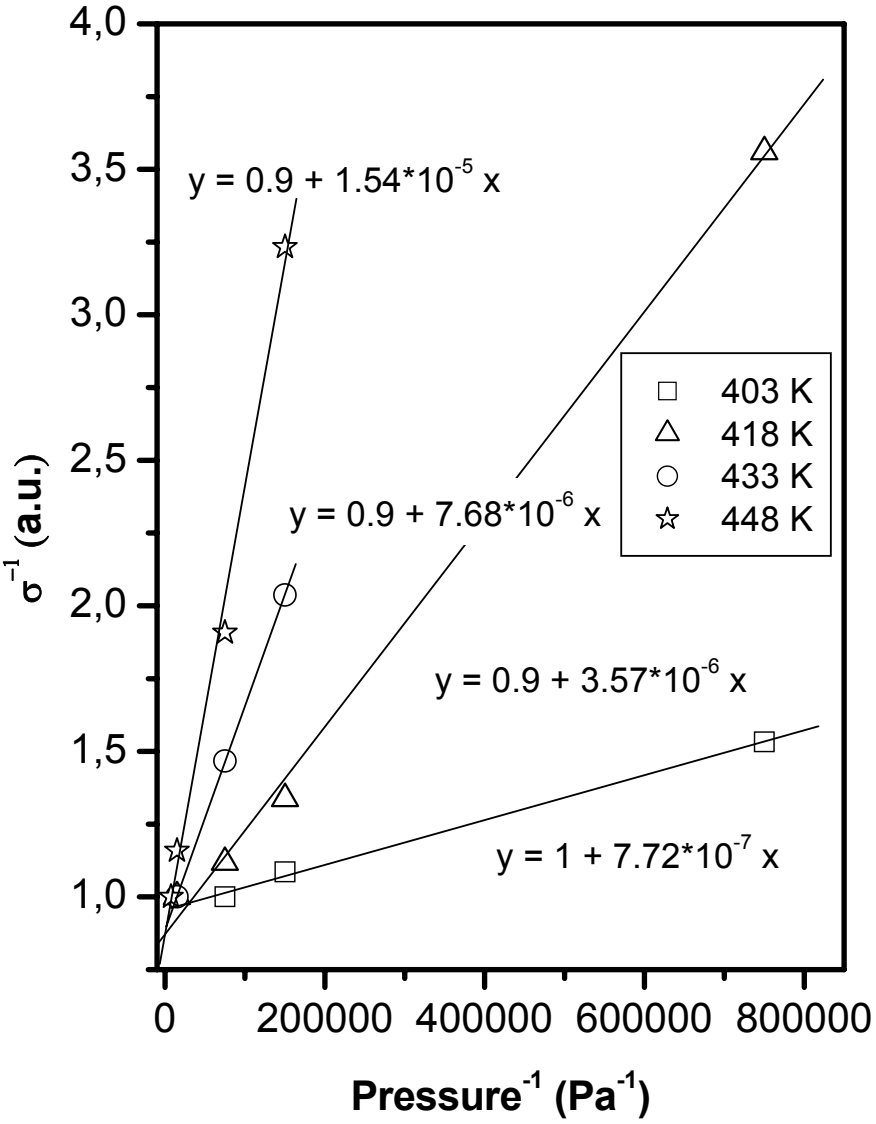

Figure 7.5. The inverse coverage of CO adsorbed on Pt(111) is plotted versus the inverse pressure. Solid lines are linear fits to experimental data.

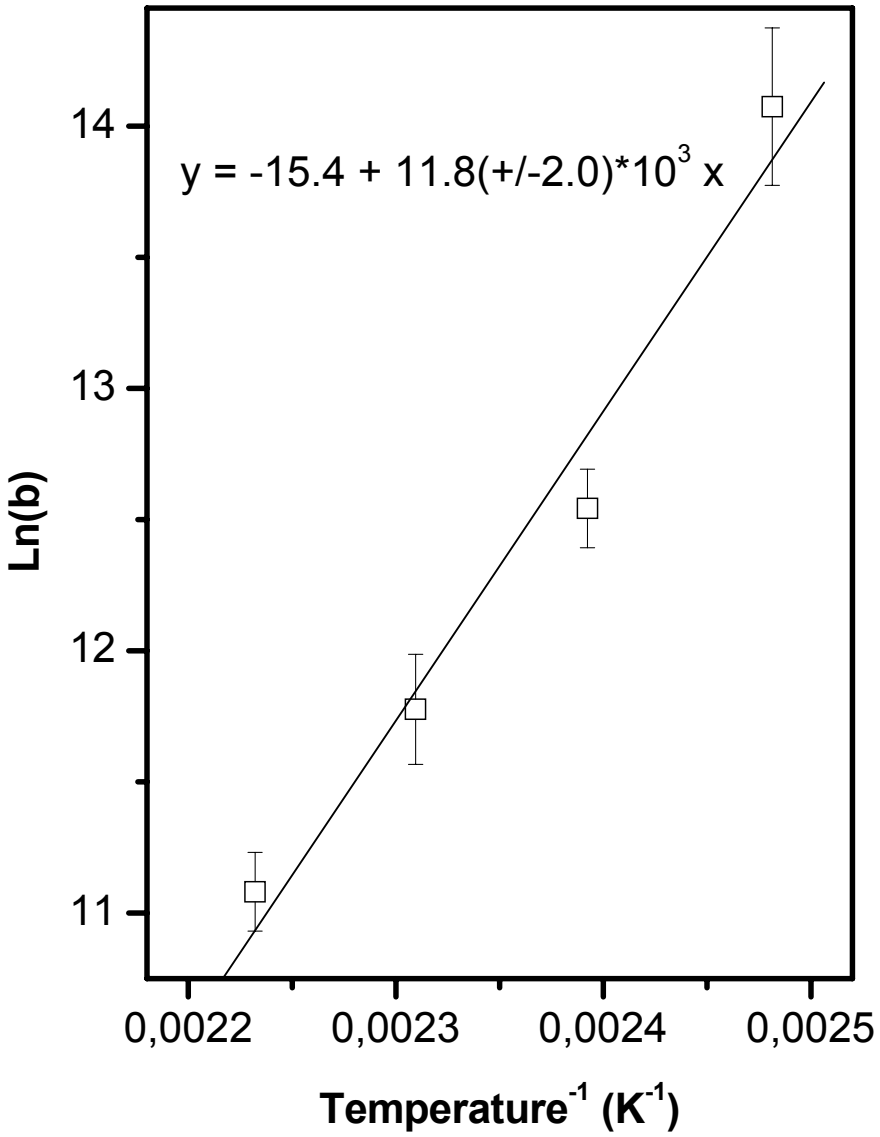

Figure 7.6. The natural logaritm of b, a parameter proportional to the exponent of the heat of adsorption is plotted against the inverse temperature. The solid line is a linear fit to the data points and the slope is the heat of adsorption of CO on Pt(111) over the gas constant, R.

illustrated in figure 3, where SFG intensity is plotted versus temperature. At lower background pressures the SFG intensity decreases more rapidly for a given temperature. CO decomposition on the Pt(111) surface can be ruled out as a reason for the decrease in SFG intensity since the signal does not change over time under temperatures and pressures used in this experiment. It has been shown that CO decomposition, at high CO pressures (40 - 400 Torr), does not take place on the Pt(111) surface below 673K. The temperature in this study is well below the temperature of decomposition for CO. [11] By analyzing the data from figure 2 a similar trend can be observed. The maximum SFG intensity appears at pressures higher than 10^{-8} Torr for temperatures above 403K. This implies that the maximum saturation coverage is not obtained until the pressure is increased enough to balance the higher desorption rate. The increasing surface coverage can be used to determine the heat of adsorption of CO on Pt(111). Once the surface has reached full coverage with 0.5 ML CO molecules in a c(4x2) structure, a further increase in pressure should lead to additional adsorption and hence a more compressed CO layer. The compression gives rise to an incommensurate layer where the CO molecules on a-top sites are displaced. This is manifested in figure 1 where the intensity of the a-top peak decreases at pressures above $5x10^{-7}$ Torr. Visible in figure 1 is also an increase in linewidth at higher pressures, which is an effect of an incommensurate layer where CO molecules are more randomly adsorbed. [19] An alternative interpretation of the decrease in SFG intensity of the CO a-top peak could be the formation of a carbonyl like Pt-$(CO)_n$ species. This would give rise to a reduction in intensity as well as a broadened linewidth. Higher temperatures should facilitate the formation of platinum carbonyls. This could explain why the decrease of the CO intensity observed in this study occurs at a lower

pressures compared to the study performed by Su et al. [8] Another trend observed from figures 2 and 3 is the change in peak positions. Stretching frequencies at 373K were around 2085 cm^{-1}. Increasing temperatures lead to a decrease in peak frequency. The frequencies observed in this study are lower than peak frequency for a-top CO on Pt(111) at room temperature, which have previously been reported to be around 2097 cm^{-1}. [20] The redshift of the a-top CO stretching frequency at higher temperatures is attributed to a shift towards the frequency of bridge bonded CO due to anharmonic coupling to a frustrated translational mode. [21,22] This shift becomes more pronounced as the temperature is increased.

The peak position also shifts with pressure. Initially it is shifted to a higher frequency when increasing the pressure. This has been shown by King et al. [23] to be due to increasing dipole-dipole coupling at higher coverages. When the pressure is increased further, the peak position is shifted back towards lower frequencies, which is in agreement with formation of an incommensurate overlayer where CO molecules are displaced from the a-top sites.

7.5. Conclusions

The pressure dependence of CO coverage on Pt(111) was studied with SFG. By relating the SFG intensity to surface coverage the heat of adsorption was determined to be 98kJ/mol, which is close agreement with previous measurements. The method of using SFG as a tool to measure thermodynamic parameters could be beneficial for in-situ measurements in pressurized or flow systems. If a specific correlation between SFG

intensity and surface coverage is obtained, this method could also be extended to studying more complex systems, such as coadsorptions.

References

(1)Yeo, Y.Y.; Vattuone, L.; King, D.A. *J. Chem. Phys.* **1997**, *106*, 392.

(2) Steininger, H.; Lehwald, S.; Ibach, H. *Surf. Sci.* **1982**, *123*, 264.

(3) Ertl, G.; Neumann, M.; Streit, K.M. *Surf. Sci.* **1977**, *64*, 393.

(4) Schweizer, E.; Persson, B.N.J.; Tüshaus, M.;Hoge, D.; Bradshaw, A.M. *Surf. Sci.* **1989**, *213*, 49.

(5) Hähner, G.; Toennies, J.P.; Wöll, C.H. *Appl. Phys. A* **1990**, *51*, 208.

(6) Olsen, C.W.; Masel, R.I.; *Surf. Sci.* **1988**, *201*, 444.

(7) Su, X.C.; Cremer, P.S.; Shen, Y.R.; Somorjai, G.A. *J. Am. Soc.* **1997**, *119*, 3994.

(8) Härle, H.; Lehnert, A.; Metka, U.; Volpp, H.-R.; Willms, L.; Wolfrum, J. *Appl. Phys. B* **1999**, *68*, 567.

(9) Härle, H.; Metka, U.; Volpp, H.**-R.;** Wolfrum, J. *Phys. Chem. Chem. Phys.* **1999**, *1*, 5059.

(10) Härle, H.; Mendel, K.; Metka, U.; Volpp, H.-R.; Willms, L.; Wolfrum, J. *Chem. Phys. Lett.* **1997**, *279*, 275.

(11) Kung, K.Y.; Chen, P.; Wei, F.; Shen, Y.R.; Somorjai, G.A.; *Surf. Sci.* **2000**, *463*, L627.

(12) Somorjai, G.A. Introduction to Surface Science and Catalysis, Wiley, New York, **1994**.

(13) Shen, Y.R. *Nature* **1989**, *337*, 519.

(14) Buck, M.; Himmelhaus, H. *J. Vac. Sci. Tech. A* **2001**, *19*, 2717.

(15) Somorjai, G.A.; Rupprechter, G. *J. Phys. Chem. B* **1999**, *103*, 1623.

(16) Bandara, A.; Katano, S.; Kubota, J.; Onda, K.; Akihide; Wada, A.; Domen, K.; Hirose, C. *Chem. Phys. Lett.* **1998**, *290*, 261.

(17) Yeo, Y.Y., Vattuone, L.; King, D.A. *J. Chem. Phys.* **1997**, *106*, 392.

(18) Ertl, G.; Neumann, M.; Streit, K.M. *Surf. Sci.* **1997**, *64*, 393.

(19) Su, X.C.; Cremer, P.S.; Shen, Y.R.; Somorjai, G.A. *Phys. Rev. Lett.* **1996**, *77*, 3858.

(20) Rupprechter, G.; Dellwig, T.; Unterhalt, H.; Freund, H.J. *J. Phys. Chem. B* **2001**, *105*, 3797

(21) Persson, B.N.J.; Rydberg, R. *Phys. Rev. B* **1985**, *32*, 3586.

(22) Persson, B.N.J.; Hoffman, F.M.; Rydberg, R. *Phys. Rev. B* **1986**, *34*, 2266.

(23) Crossley, A.; King, D. *Surf. Sci.* **1977**, *68*, 528.

Chapter 8: Conclusions

In this dissertation, high-pressure catalytic reactions were studied using sum frequency generation. The range of applications for SFG were also expanded by using the non-resonant signal to probe the electronic structure of the surface and to follow surface reactions. SFG was also employed to measure isotherms of CO adsorption on Pt(111).

The variety of data presented here shows the versatility of SFG and its strength in detecting surface adsorbates at ambient pressures between 10^{-9} Torr to 10^{3} Torr. Together with supporting techniques such as AES, LEED, TPD, gas chromatography and mass spectrometry it was possible to investigate several surface catalytic reactions.

Ammonia adsorption and dissociation was studied on clean Fe(111) and preoxidized Fe(111) under high pressure. Intermediates in the dissociation reaction were identified. Ammonia molecules have been found to dissociate at room temperature on both clean and preoxidized Fe(111) under high pressure (20 - 600 Torr). Vibrational frequencies of the associated intermediates, NH and NH_2, were identified on the clean and pre-oxidized Fe(111). Introduction of 0.5 Torr of oxygen changed the interference of the resonant and the non-resonant second order non-linear susceptibility by changing the relative phase. This can be seen as an overall lowering of the non-resonant signal and a reversal of the spectral features in the SFG spectra. Heating the surface in presence of high pressure ammonia reduces the oxygen coverage and there is another relative phase change of 180° to restore the initial spectral features.

It was found that the magnitude of the non-resonant SFG intensity could be used to follow surface reactions, such as adsorption, oxidation and reduction. Adsorption on

Fe(111) causes a distinct change in the SFG signal and a correlation between the work function change and magnitude of the non-resonant SFG signal is proposed. Knowing the effect on work function upon adsorption, the change of non-resonant SFG signal can be predicted. The change in SFG non-resonant signal can be used to follow surface reactions, including iron oxidation, ammonia dissociation and nitride formation on iron surfaces as well as reduction of iron oxides. It was also found that Fe(111) has a strong non-resonant SFG signal. The change in non-resonant SFG intensity upon tuning of the exciting energy is associated with the detailed surface electronic structure of Fe(111).

The second high-pressure reaction presented in this dissertation is ethylene hydrogenation on Pt(111) and especially the effect of CO poisoning on this reaction. It was discovered that when CO adsorbed on the ethylidyne pretreated surface, its vibrational spectra red- shifted about 75 cm^{-1}, which was mainly due to the weakening of the CO bond through d-π back donation from coadsorbed ethylidyne molecules. In the CO pretreated Pt(111) surface, the presence of high pressure ethylene did not change the vibrational spectra in the CH stretching region indicating that ethylene cannot adsorb on the surface that is covered by a monolayer of CO.

During the studies of catalytic ethylene hydrogenation in the presence of CO, it was found that CO poisons the catalytic reaction by site blocking up to 400K where CO desorbs from the Pt(111) surface. The measured apparent activation energy was 20.5 kcal/mol instead of 10 kcal/mol.

The pressure dependence of CO coverage on Pt(111) was studied with SFG. By relating the SFG intensity to surface coverage, the heat of adsorption was determined to be 98kJ/mol, which is close agreement with previous measurements. The method of using

SFG as a tool to measure thermodynamic parameters could be beneficial for in-situ measurements in pressurized or flow systems. If a specific correlation between SFG intensity and surface coverage is obtained, this method could also be extended to studying more complex systems, such as coadsorptions.